Biomaterials Science

REVIEW

View Article Online
View Journal | View Issue



Cite this: *Biomater. Sci.*, 2018, **6**, 746

# Recent progress in the development of near-infrared organic photothermal and photodynamic nanotherapeutics†

Houjuan Zhu, Penghui Cheng, Peng Chen and Kanyi Pu *

Received 29th December 2017,
Accepted 5th February 2018

DOI: 10.1039/c7bm01210a

rsc.li/biomaterials-science

Phototherapies including photothermal therapy (PTT) and photodynamic therapy (PDT) have gained considerable attention due to their high tumor ablation efficiency, excellent spatial resolution and minimal side effects on normal tissue. In contrast to inorganic nanoparticles, near-infrared (NIR) absorbing organic nanoparticles bypass the issue of metal-ion induced toxicity and thus are generally considered to be more biocompatible. Moreover, with the guidance of different kinds of imaging methods, the efficacy of cancer phototherapy based on organic nanoparticles has shown to be optimizable. In this review, we summarize the synthesis and application of NIR-absorbing organic nanoparticles as phototherapeutic nanoagents for cancer phototherapy. The chemistry, optical properties and therapeutic efficacies of organic nanoparticles are firstly described. Their phototherapy applications are then surveyed in terms of therapeutic modalities, which include PTT, PDT and PTT/PDT combined therapy. Finally, the present challenges and potential of imaging guided PTT/PDT are discussed.



## 1. Introduction

Phototherapies, including photodynamic therapy (PDT) and photothermal therapy (PTT), have gained much attention due to their attractive non-invasiveness nature for cancer therapy.[1–3] The process of cancer phototherapy mainly includes delivery of a phototherapeutic agent to tumors and subsequently irradiation of the treated tumor site with specific light. PTT, as one category of phototherapy, employs a photothermal agent to convert the absorbed photon energy into heat, directly ablating cancer cells with minimal invasion to surrounding healthy tissues.[4–9] Different from PTT, PDT mainly utilizes photosensitizers to be excited with light of an appropriate wavelength for converting molecular oxygen into cytotoxic reactive oxygen species (ROS), such as singlet oxygen ($^1O_2$), which in turn damages cancer cells through oxidative stress and consequently induces cell death.[10–13] With inherent non-toxicity in the dark and light-induced toxicity of these nanoagents, phototherapies emerge with excellent spatial specificity and noninvasiveness over the traditional chemotherapy and radiotherapy.[14,15]

In optical imaging and phototherapy for both superficial and deep malignant tissues, near infrared (NIR) light has the advantages of maximum penetration depth and minimum autofluorescence of biological species in the NIR spectrum in contrast to UV/visible light.[16,17] Many NIR-absorbing nanomaterials have recently been synthesized as effective nanoplatforms to integrate chemistry, biology, bioinformatics, medical physics and various other functions to overcome various problems in traditional cancer diagnosis and therapy. However, as far as we are concerned, existing inorganic nanomaterials, such as gold nanostructures,[18–20] silver nanoparticles,[21,22] palladium nanoparticles,[23,24] metal sulfide nanoparticles,[25–28] two dimensional materials,[29–32] oxide nanoparticles[33–37] and carbon derivatives,[38–41] usually have some disadvantages including non-biodegradability and long retention time in the body that could potentially increase their probability of long-term toxicity. In contrast, organic nanomaterials have the superiority for biological applications because of their biocompatibility, size-independent optical properties and structural versatility. In general, the different optical properties of NIR-absorbing organic nanoparticles are obtained through encapsulating different organic chromophores into nanoparticles, allowing them to have versatile ability in different imaging tasks. Unlike inorganic nanomaterials that possess size-dependent optical properties, organic nanoparticles have size-independent photophysical properties, making them feasible to develop nanoparticles with the ability of multiplexed imaging at different wavelengths with similar pharmacokinetic properties.[42–45] Moreover, the common PEGylation or biocompatible polymer encapsulation of NIR-absorbing organic com-

*School of Chemical and Biomedical Engineering, Nanyang Technological University, 70 Nanyang Drive, 637457, Singapore. E-mail: kypu@ntu.edu.sg*

†Electronic supplementary information (ESI) available. See DOI: 10.1039/c7bm01210a

ponents passivates their surface, resulting in ideal dynamic biodistribution in living animals as well as long-term circulation and effective accumulation of nanoparticles at the tumor site. Due to their excellent light-harvesting and light-amplifying capability, NIR-absorbing organic materials, such as cyanine dyes,[46–48] porphyrin derivatives[49,50] and semiconducting polymers (SPs),[51–59] have been extensively applied to both *in vitro* and *in vivo* imaging and real-time diagnostics. In addition to imaging, the excellent photoconversion efficiency of NIR-absorbing organic materials to generate heat or toxic ROS, including $^1O_2$, superoxide anions, and hydroxyl radicals, further proves their feasibility in PTT and PDT.

Research and publications regarding the development of photothermal and photodynamic nanoagents are increasing in number, and the design and biomedical applications of photothermal and photodynamic inorganic nanotheranostics have been nicely summarized in a number of reviews.[43,60–65] The recent development and applications of NIR organic nanotheranostic agents are summarized and compared in Table 1 in the ESI.† This review mainly focuses on the recent progress of NIR-absorbing organic nanomaterials for cancer phototherapy. In the following, the chemistry and *in vivo* applications of photothermal and photodynamic agents based on NIR-absorbing organic nanoparticles are introduced first, which is followed by the discussion of the combined photothermal/photodynamic systems. Finally, a summary and an outlook are given along with the discussion of the current challenges and perspectives of phototherapy in biology and medicine.

## 2. Photothermal nanotherapeutics

Because of their poor water solubility and weak tumor targeting ability, these free NIR-absorbing organic materials such as NIR dyes and SPs were generally encapsulated into proteins or conjugated with amphiphilic polymers to form NIR-absorbing organic nanoparticles, so that both these disadvantages could be overcome and their accumulation at the tumor site could also be improved. Recently, a large amount of NIR-absorbing organic nanoparticles including NIR dye based nanoparticles[66–68] and semiconducting polymer nanoparticles (SPNs)[69–71] have been explored as therapeutic agents for PTT and achieved highly promising results in several animal models.[72] The photothermal conversion efficiency of NIR organic nanoagents is summarized and compared in Table 2 in the ESI.† For example, Huh and Haam's group developed a novel organic photothermal nanoagent based on polyaniline (PANPs) for cancer-cell ablation.[73] PANPs exhibited high NIR absorbance in an intracellular environment, where the pH value is acidic and oxidative species exist. Thus, under NIR irradiation, the organic PANPs could result in effective ablation of cancer cells. Similarly, Li and Ma's group also fabricated a polyaniline based photothermal agent by coating with polyoxyethylene chains (F-PANPs).[74] The F-PANPs exhibited strong NIR absorbance and high photothermal conversion efficiency and thus could lead to efficient PTT of tumor-bearing mice. Additionally, Liu's group developed poly(vinyl alcohol) (PVA)-stabilized polypyrrole (PPy) nanoparticles through a microemulsion method using $Fe^{3+}$ as the catalyst and PVA as the stabilizer.[75] Owing to its high NIR absorbance between 700 and 1200 nm, this PPy nanoparticle could achieve 100% tumor elimination through PTT. In addition, a series of novel PTT nanoagents based on semiconducting polymers have recently been designed to exhibit high photothermal conversion efficiency and to realize highly efficient *in vivo* tumor PTT.[76–81]

### 2.1. Imaging guided photothermal nanotherapeutics

Due to some disadvantages including insufficient visualization towards delivery, distribution, metabolism and digestion of PTT agents, and a lack of precise and comprehensive evaluation of PTT outcome towards tumor tissues, applications of PTT in clinics were seriously limited. The combination of PTT and imaging could not only identify the location, shape, size and type of tumor, but also real-time monitor therapeutic effects, enhance therapy efficiency and reduce side effects. Recently, several imaging techniques, such as near infrared fluorescence (NIRF) imaging, photoacoustic (PA) imaging, magnetic resonance (MR) imaging, have been explored to guide PTT based on NIR-absorbing organic nanoparticles.

**2.1.1. Single-modal optical imaging guided PTT.** Conventionally, NIR-absorbing organic nanoparticles could commonly be applied as NIRF imaging agents owing to the fact that chromophores could absorb external light with a specific wavelength. Thereinto, a number of NIR-activatable organic nanotheranostics based on SPs and conventional NIR dyes, such as 3-(4-carboxybenzyl)-2-((*E*)-2-((*E*)-3-((*E*)-2-(3-(4-carboxybenzyl)-1,1-dimethyl-1,3-dihydro-2*H*-benzo[*e*]indol-2-ylidene)ethylidene)-2-chlorocyclohex-1-en-1-yl)vinyl)-1,1-dimethyl-1*H*-benzo[*e*]indol-3-ium bromide (IR825),[82,83] 2-[2-[2-chloro-3-[(1,3-dihydro-3,3-dimethyl-1-propyl-2*H*-indol-2-ylidene)ethylidene]-1-cyclohexen-1-yl]ethenyl]-3,3-dimethyl-1-propylindolium (IR780),[84–90] and indocyanine green (ICG),[91,92] have proved promising in NIRF imaging-guided PTT of tumors in living mice. For example, Liu's group developed NIR dye (IR825) based nanotheranostic agents for NIRF imaging guided PTT through the encapsulation of PEG and HSA, respectively.[82,83] Under NIR laser irradiation, these nanotheranostic agents exhibited excellent imaging-guided PTT in an animal tumor model.

Recently, because of its advantages of deeper tissue penetration, higher spatial resolution and better tissue contrast, PA imaging has emerged as a new nonionizing imaging technology, which can be widely applied in visualizing anatomic and physiological changes in diseases.[31,93–97] The combination of PTT with PA imaging allows for a simple approach towards enhanced accuracy of cancer diagnosis and improved therapy efficacy.[98] Tang *et al.* designed an organic small molecule (TPA-T-TQ) with intensive absorption in the NIR window, which was further fabricated to be an effective biocompatible phototheranostic nanoagent with photobleaching/reactive oxygen and nitrogen species (RONS) resistances for PA imaging-guided PTT.[99] Additionally, novel pH responsive PA

imaging guided PTT based on NIR dyes was developed. For example, Liu's group and Smith's group, respectively, designed a NIR croconine- and its derivative-based nanoparticle for real-time ratiometric PA imaging of pH in the tumor, and also for pH responsive PTT of tumors under NIR laser irradiation.[100,101] Also, a novel kind of porphysome-based nanotheranostic agent was fabricated through conjugating porphyrin to phospholipid and transforming porphyrin–phospholipid conjugates into nanovesicles *via* supramolecular self-assembly.[50] This nanotheranostic agent was composed of highly packed porphyrin bilayers, which could induce strong self-quenching *via* an intermolecular interaction, leading to photothermal effects and consequently PA properties. Following systemic administration, this porphysome-based nanotheranostic agent enabled sensitive PA imaging of tumors in xenograft-bearing mice, and induced photothermal tumor ablation under NIR laser irradiation, exhibiting the potential of organic nanoparticles for biophotonic imaging guided phototherapy. Similarly, a supramolecular strategy of peptide-modulated self-assembly of photoactive porphyrins was developed to fabricate photothermal nanodots.[102] In this system, the J-aggregates of nanodots induced by self-assembling nature of porphyrins totally quenched fluorescence and inhibited $^1O_2$ generation, leading to a high photothermal conversion efficiency and thus a PA signal. The nanodots were successfully applied in photothermal acoustic imaging and anti-tumor therapy. These investigations have provided useful guidelines for the development of NIR dye-based nanoagents in imaging-guided PTT.

Moreover, due to a unique set of advantages including high absorption coefficients, controllable dimensions, high photostability and good biocompability, SPNs have been widely reported to show promising PA imaging-guided photothermal cancer ablation both *in vitro* and *in vivo*.[44,56,57,94,95,103–106] For instance, a terrylenediimide (TDI)-poly(acrylicacid) (TPA)-based nanomedicine (TNM) platform was reported as an intrinsic theranostic agent for efficient PA imaging-guided tumor PTT.[107] Pu *et al.* designed a binary theranostic SPN with both enhanced PA brightness and higher PTT efficiency through an intraparticle molecular orbital engineering approach, allowing for amplified theranostics in living mice.[108] Within this theranostic SPN, a SP, poly[2,6-(4,4-bis(2-ethylhexyl)-4*H*-cyclopenta-[2,1-*b*;3,4-*b*']dithiophene)-*alt*-4,7-(2,1,3-benzothiadiazole)] (PCPDTBT) and an optical dopant, (6,6)-phenyl-C71-butyric acid methyl ester (PC70BM), served as an electron donor and acceptor, respectively. Photoinduced electron transfer (PET) favored by an energy alignment between the two optical components induced fluorescence quenching and enhanced non-radiative heat generation under laser irradiation, consequently resulting in both enhanced PA brightness and improved PTT

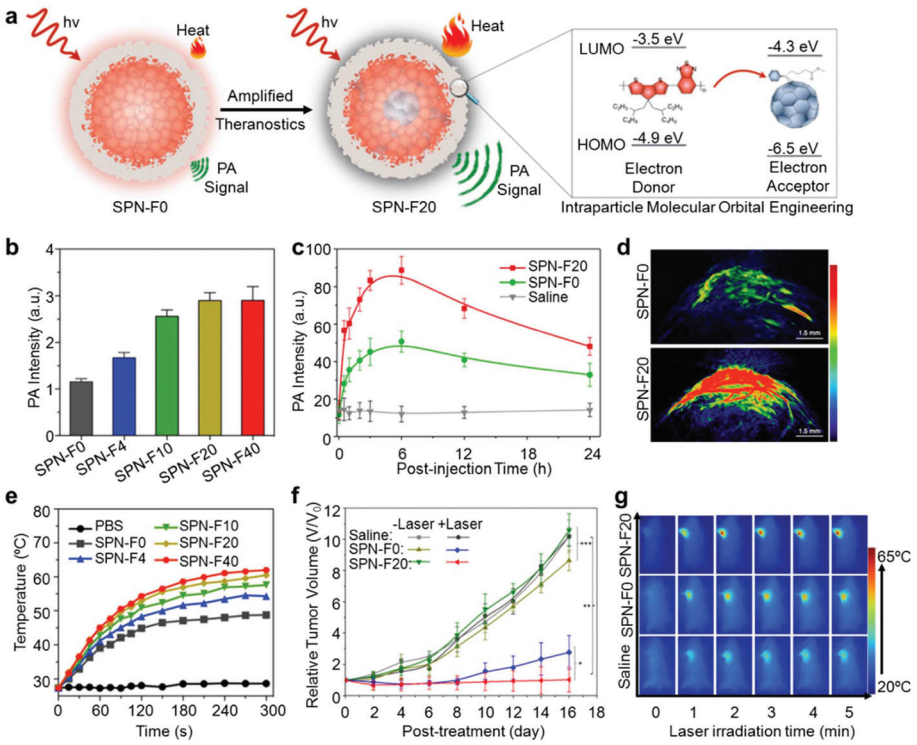


**Fig. 1** SPNs for PA imaging guided PTT. (a) A schematic illustration of the design of theranostic SPNs for amplified PA imaging and PTT. (b) Quantification of PA intensities of different SPNs in solutions. (c) PA intensities at 750 nm as a function of time after administration of SPNs or saline. (d) PA images of a tumor treated with SPNs 6 h after systemic administration. (e) The temperature curve *versus* laser irradiation time of SPNs in solutions. (f) Changes in the tumor size of mice after different treatments. (g) IR thermal images of 4T1 tumor-bearing mice under 808 nm laser irradiation (0.3 W cm$^{-2}$) after injection of saline or SPNs for 6 h. Reproduced from ref. 108 with permission from American Chemical Society.

 

efficiency (Fig. 1a). As confirmed by *in vitro* histological data, both the PA intensity and photothermal efficiency of SPNs increased gradually with the PC70BM doping amount, and reached the maximum when the amount of PC70BM reached 20 w/w% (SPN-F20), where the PA signal and temperature were 2.6 and 1.3-fold, respectively, higher than those of the SPNs without doping (SPN-F0) upon laser irradiation (Fig. 1b and e). After systemic administration, compared with SPN-F0, the tumor PA signal for SPN-F20-injected mice was always higher at any time point, and was 1.8-fold higher at 6 h post-injection when it reached the maximum (Fig. 1c and d). In addition, upon 808 nm laser irradiation for 5 min, the tumor temperature of mice treated with SPN-F20 was higher than that of SPN-F0-injected mice at each time point (Fig. 1f). The better capability of SPN-F20 to inhibit tumor growth was shown for at least 2 weeks (Fig. 1g). The result indicated that the utilization of SPNs with PC70BM doping as a phototheranostic agent could enhance PA imaging and improve photothermal ablation of tumors in living mice. Thus, the organic optical theranostics based on SPNs hold great promise for merging light-intensive imaging with therapeutic applications.

Similarly, Liu's group fabricated semiconducting oligomer based nanoparticles with strong NIR absorbance for PA imaging of sentinel lymph nodes, and tumor PTT.[109] This group further designed a set of SPNs with different electron acceptors (A) and a planar electron donor (D), in which the D–A strength could affect their absorption, emission, extinction coefficient, and ultimately PA and PTT performance.[110] Zhang and Li's group synthesized a series of acceptor–π–acceptor (A1–π–A2) type SPs, in which diketopyrrolopyrrole (DPP) and thiophene served as the A1 electron accepting block and π-bridge, and A2 was variable and mainly responsible for their PTT and PA imaging performances.[111] The SP based nanotheranostic agents with PEGylation exhibited efficient PA imaging guided PTT both *in vitro* and *in vivo*. A similar thiophene–benzene–diketopyrrolopyrrole (TBD)-based polymer with a photothermal conversion efficiency of 68.1% was also applied as an excellent therapeutic agent for PA imaging-guided PTT.[112] Therefore, it may be meaningful to develop different nanostructures of SPN based nanotheranostic agents with excellent imaging performance for applications in PTT.

**2.1.2. Single-modal morphological/anatomical imaging guided PTT.** In the recent years, versatile and traditional morphological/anatomical imaging techniques, including MR imaging,[113–116] ultrasound (US) imaging[117–119] and X-ray-computed tomography (X-ray CT) imaging,[120–123] have been extensively applied for medical imaging due to a series of advantages, such as high spatial resolution, real-time response, and noninvasiveness and non-radiation features. The combined PTT and MR/US/CT imaging nanoagents could greatly enhance therapeutic efficacy and reduce side effects, consequently leading to extensive applications of imaging-guided localized hyperthermia treatment induced by NIR light.

Manganese ($Mn^{2+}$) compounds and gadolinium ($Gd^{3+}$) chelates are the most frequently employed contrast agents for MR imaging. In this regard, Liu's group fabricated nanoscale metal–organic particles (Mn-IR825 NMOPs) with a shell of polydopamine (PDA) and further PEGylation to achieve highly efficient MR imaging-guided PTT for tumors on the mice model, and NMOPs were composed of $Mn^{2+}$ as the MR imaging contrast agent and a NIR dye (IR825) as the PTT agent.[116] Additionally, Lu *et al.* fabricated a new generation of photothermal therapeutic agents based on biopolymer dopamine–melanin colloidal nanospheres (Dpa–melanin CNSs) and further used Gd-diethylenetriamine pentaacetic acid (DTPA) to modify Dpa–melanin CNSs for their applications in MR imaging-guided phototherapy of tumors *in vivo*.[124] Similarly, Haam and Huh's group reported $Gd^{III}$-loaded polyaniline (PANI)-based photothermal submicronic particles (GPAPs).[125] In these nanoparticles, acid anhydrides of diethylenetriaminepentaacetic dianhydride (DTPA-DA) were conjugated with PANI using carbodiimide and then were chelated as well as reduced the potential toxicity of $Gd^{III}$, and further modified GPAPs using an anti-epidermal growth factor receptor (EGFR) called cetuximab (CET) as a targeting moiety (CET-GPAPs) (Fig. 2a). In the presence of $Gd^{III}$ in this system, the contrast performance in $T1$-weighted spin echo MR images was observed to be 8-fold higher than that of a commercial imaging agent (Dotarem) (Fig. 2b). Due to the high NIR absorption of PANI in GPAPs, the GPAP solution exhibited a significant temperature increment compared to distilled water upon NIR laser irradiation (Fig. 2c). *In vivo* MR imaging of EGFR+ tumors in living subjects was conducted on mice with subcutaneous A-431 cell xenografts (Fig. 2d). MR signals of CET-GPAPs at the tumor sites increased to a greater extent than in the mice injected with IgG-GPAPs, indicating that a much larger amount of $Gd^{III}$ in CET-GPAPs was delivered to tumor sites than IgG-GPAPs. Subsequently, the high photothermal ablation efficiency of the GPAPs to treat epithelial cancer both *in vitro* and *in vivo* was verified in a xenograft model – mice were injected with A-431 cells at 6 h post-injection (Fig. 2e). These results highlighted the capability of specific target-delivery and exceptional therapeutic efficacy of CET-GPAPs. As some MRI agents could be chelated onto the surface of SPNs, more advanced theranostic probes containing bioactive molecules could be developed for on-demand drug release and thermal-activation monitoring of metabolic pathways by MRI.

NIR-absorbing organic nanoparticles have also been successfully studied as US contrast agents for tumor PTT. For example, Dai's group constructed water-dispersible PPy nano-/microcapsules with a soluble PPy complex as US imaging-guided photothermal agents for tumor ablation using versatile oil-in-water emulsion methods.[118] In this work, because of the encapsulated liquid perfluorooctylbromide (PFOB) and high NIR absorbance of the PPy shell, the obtained PPy capsules could trigger photothermal ablation of tumor cells guided by US imaging, with no significant side effects under NIR laser irradiation. In addition to single-modal imaging guided PTT, multi-modal imaging-guided PTT nanoagents, which are constructed by combining multi-functional imaging reagents into a single PTT nanoplatform, have been investigated recently to

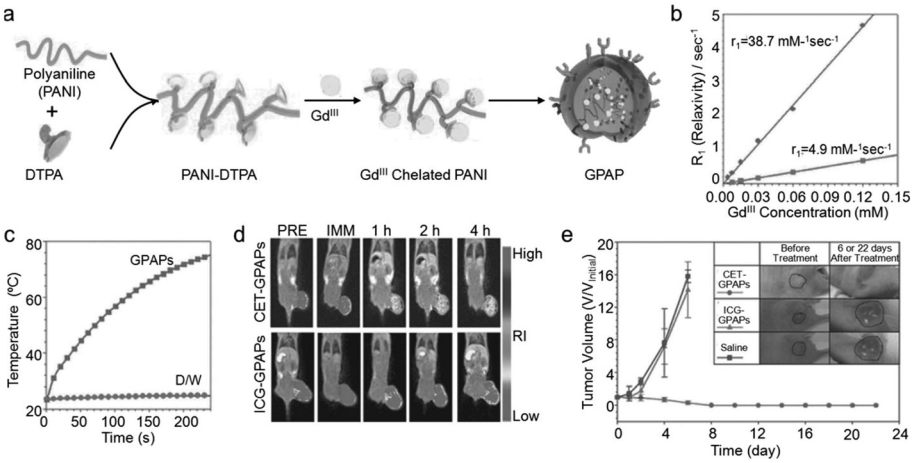


Fig. 2 Gd$^{III}$-Loaded polyaniline nanoparticles (GPAPs) for MR imaging-guided PTT. (a) A schematic illustration of preparing Gd$^{III}$-loaded polyaniline nanoparticles for PTT. (b) The relaxivity ($R1$) graph *versus* various concentrations of GPAPs and a commercial contrast agent (doratem). (c) Photothermal effects of GPAPs under NIR laser irradiation for 4 min (5 W cm$^{-2}$). (d) MR images of epithelial tumor bearing mice injected with CET-GPAPs or IgG-GPAPs during the 4 h evaluation period. (e) Changes in tumor volumes after treatment with CET-GPAPs, IgG-GPAPS, or saline as a control. Reproduced from ref. 125 with permission from WILEY-VCH.

satisfy the comprehensive and precise tumor identification. Consequently, some NIR-absorbing organic photothermal nanoagents with both superior photothermal conversion efficacy and unexpected imaging properties have been developed.

**2.1.3. Multimodal imaging guided PTT.** Compared to single modality, multimodal imaging has a higher probability to fulfil the increasing demands in advanced biotechnology. Although PA imaging has some advantages over fluorescence imaging, it is preferred in theranostic medicine to develop a combination of PA with other medical imaging techniques. For example, Li and Yan's group for the first time fabricated a stimuli-responsive tumor-targeting rapamycin/DiR loaded lipid-polyaniline nanoparticle (RDLPNP) for enhanced dual-modal imaging-guided PTT.[126] In this system, polyaniline (PANI) with a π–π electronic conjugated structure served as both a PTT agent and an appropriate model receptor of fluorescence resonance energy transfer (FRET) for PA imaging; the loaded cyanine probe (1,1-dioctadecyl-3,3,3,3-tetramethylindotricarbocyanine iodide, DiR) served as a donor for NIRF; and rapamycin (RAPA) was used as the anti-angiogenesis chemotherapeutic agent. After intravenous injection of RDLPNPs into HeLa tumor bearing mice, NIRF and enhanced PA (from DLPNPs) signals were obviously observed at the tumor region over time, and an enhanced anti-tumor effect from combined chemo-photothermal therapy was observed. In another example, Sun and Zhang's group developed polyethylene glycol (PEG) modified croconaine dye (CR780) for PA/NIRF imaging-guided PTT.[127] Similar designs of heptamethine Cy-containing polymer (CyP) based nanoparticles were also reported by Xie's group.[128] Additionally, holo-Tf-indocyanine green (holo-Tf-ICG) nanoassemblies and cyanine dye IR808-conjugated hyaluronic acid nanoparticles (HAIR NPs) were, respectively, prepared by using a one-step method for NIRF and PA dual-modal imaging guided PTT of gliomas and tumors by Zheng's group and Cai's group.[129,130] With these nanoparticles, they achieved simultaneous NIRF and PA imaging guided photothermal ablation of xenografted tumors *in vivo*. Wang and Liang's group fabricated a triple-modal X-ray CT, NIRF and PA imaging guided PTT nanotheranostic agent based on activatable hyaluronic acid (HA) conjugating two NIR dyes of Cy5.5 and IR825 and encapsulating perfluorooctylbromide (PFOB).[131] Besides the conventional combined imaging modal of NIRF and PA imaging, a recent research showed that PEGylated polypyrrole nanoparticles conjugating gadolinium chelates (Gd-PEG-PPy NPs) could be used for dual-modal MR/PA imaging guided PTT of cancer.[51] In another example, Cai *et al.* also designed ICG-loaded polydopamine (PDA)-iron ion ($Fe^{3+}$) coordination nanoparticles (PDA-$Fe^{3+}$-ICG) as a nanotheranostic system with strong NIR absorption for PA and MR dual-modal imaging-guided cancer PTT treatment.[132] A metal–organic framework MIL-100(Fe) based nanotheranostic agent (MOF@HA@ICG NPs) comprising hyaluronic acid (HA) and ICG was successfully developed for NIRF imaging-guided PTT.[133]

NIRF imaging guided PTT combined with MR imaging or CT imaging has also been developed recently. For instance, Liu *et al.* reported a HSA-Gd-IR825 nanocomplex based on a NIR dye (IR825) and human serum albumin (HSA) linked with DTPA molecules and further chelated gadolinium for dual-modal NIRF and MR imaging guided PTT of metastatic cancer cells.[134] Multifunctional micelles loaded with a NIR dye and labeled with radionuclide rhenium-188 ($^{188}$Re) as well as indium-111 ($^{111}$In) radiolabeled IR780/micelles conjugated with cetuximab micelles (cetuximab/IR780/micelles) were fabricated for NIRF and single photon emission computed tomography (microSPECT) imaging guided photothermal ablation of cancer by Shieh's group.[135,136] In a word, our study high-

 

lights the great potential of NIR-absorbing nanotheranostics with multimodal imaging properties for enhanced tumor PTT.

### 2.2. Chemo-photothermal nanotherapeutics

Generally, single-modality PTT could not completely destruct cancer cells and may result in the survival of the residual cells after photothermal treatment. This incomplete tumor eradication therapy could cause tumor regrowth in the long term. Photothermal effects were reported to have the ability to facilitate intracellular translocation of anti-cancer drugs for enhanced chemotherapy. Thus, in order to further improve cancer therapy efficacy, several types of theranostic platforms have been developed to combine chemotherapy and PTT together.

For instance, Yin and Nie's group reported an *in vivo* multimodal imaging-guided chemo-photothermal integrated nanotheranostic agent, which consisted of IR780 and camptothecin (CPT) encapsulated in poly(ε-caprolactone) (IR780/CPT@PCL) as the core and helical poly(phenyl isocyanide) (PPI) blocks as the shell with pH-responsive rhodamine B (RhB).[137] When irradiated with a NIR laser, the release of CPT was significantly improved from the core by the heat generated, triggering synergetic chemo-photothermal therapy and decreasing tumor recurrence rates in mice. Simultaneously, the fluorescence of the pH-responsive RhB moieties could significantly increase when pH changes from 7.4 to 5.5. IR780 could generate strong PA signals owing to its high absorption coefficient. Thus, these multifunctional micelles showed excellent NIRF/PA imaging guided photothermal tumor ablation.

Shieh and Peng's group designed a novel PTT nanoagent, DOX@Cy micelle, based on a novel amphiphilic copolymer, methoxy poly(ethylene glycol) (mPEG)-cyanine-poly(ε-caprolactone) (PCL) (mPEG-Cy-PCL), for simultaneous drug delivery and NIRF imaging-guided PTT.[138] In this system, doxorubicin (DOX) and mPEG-Cy-PCL were, respectively, applied to generate a chemotherapeutic effect and a thermal effect under NIR light irradiation. Under NIR laser irradiation, the micelles could be destroyed by the heat generated from the photothermal effect, and thus rapidly release a single dose of DOX, confirming the occurrence of photothermally controlled drug delivery. Therefore, the enhanced antitumor efficacy *in vitro* and *in vivo* was realized through the synergistic chemo-photothermal therapeutic effects. Similarly, Zhao and Korzh's group developed a multifunctional PTT nanoplatform based on a DOX conjugated amphiphilic block copolymer with a terminal folic acid moiety encapsulating the IR825 dye (PDOX/IR825 nanoparticles) for combined chemo-photothermal therapy.[139] The encapsulated IR825 dye could act as a NIRF contrast and PTT agent due to its high NIR absorbance. The conjugated DOX could be released quickly under weak acidic conditions because of the cleavage of the acid-labile hydrazone bond. Under NIR light irradiation, higher therapeutic efficacy of PDOX/IR825 nanoparticles was confirmed *in vitro* and *in vivo* through the combined chemo-photothermal therapy. In another example, a simple chemo-photothermal nanotheranostic agent comprising DOX and ICG loaded poly(lactic-*co*-glycolic acid) (PLGA)-lecithin-PEG (DINPs) was fabricated using a single-step sonication method by Cai's group.[140] Some similar nanotheranostic agents that combined DOX and ICG have also been reported for imaging guided chemo-photothermal therapy.[141,142]

Besides this, Liu's group reported a novel "abraxane-like" nanotheranostic agent for NIRF imaging-guided chemo-photothermal therapy of cancer. A NIR dye (ICG) could be easily self-assembled with the albumin protein HSA and paclitaxel (PTX), leading to the formation of stable nanoparticles (HSA–ICG–PTX) (Fig. 3a).[143] In this system, HSA and PTX, respectively, acted as a biocompatible carrier platform and an effective antitumor drug, while the NIR dye ICG served as both a fluorescence imaging probe and a photothermal agent. Due to the

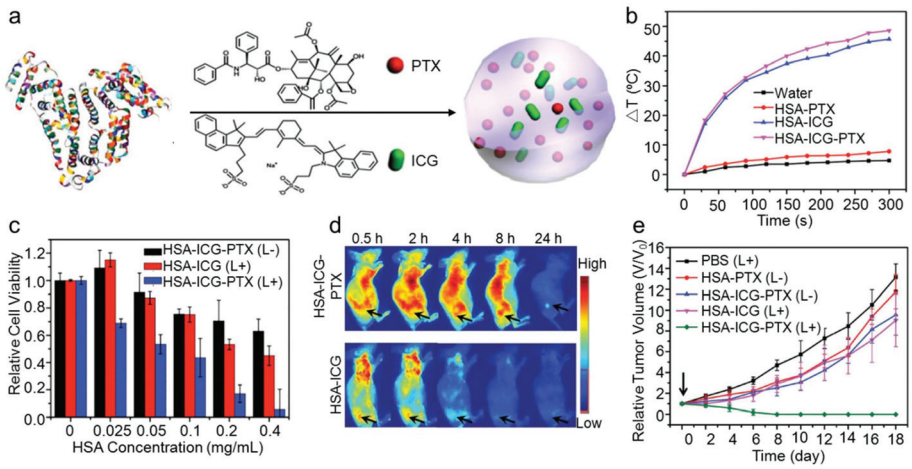


**Fig. 3** Self-assembled HSA–ICG–PTX nanoparticles for chemo-photothermal therapy. (a) A schematic illustration of the formation of HSA–ICG–PTX nanoparticles. (b) Temperature curves of different solutions under 808 nm laser irradiation (0.5 W $cm^{-2}$). (c) *In vitro* cytotoxicity and photocytotoxicity of HSA–ICG and HSA–ICG–PTX. (d) *In vivo* fluorescence images of 4T1 tumor-bearing nude mice up to 24 h after intravenous injection of HSA–ICG–PTX or HSA–ICG. (e) Changes in tumor sizes in different groups of mice after various treatments. Reproduced from ref. 143 with permission from WILEY-VCH.

strong NIR absorbance of ICG, HSA–ICG–PTX showed photothermal efficiency similar to HSA–ICG upon NIR laser irradiation (Fig. 3b). To investigate the *in vitro* therapeutic effect of HSA–ICG–PTX, the treatment effect was examined quantitatively by a MTT assay on 4T1 cells, showing that more effective cancer cell death could be induced by HSA–ICG–PTX with laser irradiation in comparison with either HSA–ICG–PTX without laser exposure or simple HSA–ICG under NIR laser irradiation (Fig. 3c). *In vivo* NIRF imaging was performed on the 4T1-xenograft tumor model after intravenous injection of HSA–ICG–PTX and HSA–PTX (Fig. 3d). Compared with the HSA–ICG complex, HSA-ICG–PTX nanoparticles exhibited a prolonged blood circulation due to the enlarged particle size and enhanced complex stability in HSA–ICG–PTX to slow down renal excretion of ICG. Additionally, HSA–ICG–PTX nanoparticles were injected intravenously into tumor-bearing nude mice for chemo-photothermal therapy (Fig. 3e). Tumors on mice treated with chemotherapy alone (HSA–PTX, HSA–ICG–PTX without laser) or PTT alone (HSA–ICG with laser) were moderately inhibited in the first few days, while tumors on mice treated with HSA–ICG–PTX were completely eliminated without any regrowth in the period after NIR laser irradiation. These results demonstrated that HSA–ICG–PTX exhibited excellent synergistic therapeutic effects of the combined PTT and chemotherapy. In addition to this system, this group also fabricated nano-assemblies of J-aggregates based on the NIR dye IR825 for the combined photothermal-chemotherapy of cancer, in which IR825 was firstly complexed with the low-molecular-weight cationic polymer PEI, followed by modifying PEG and loading DOX.[144] This investigation demonstrates the promise of those NIR dye based organic nanoparticles in imaging-guided combined therapy of cancer.

SPNs have recently been used as both drug nanocarriers and PTT agents for chemo-phototherapy of tumors in living animals.[145–147] For example, Pu's group recently reported a simplified theranostic nanoagent (DSPN5) for NIRF/PA imaging guided chemo-photothermal therapy with multifunctionality based on an amphiphilic semiconducting polymer (PEG-PCB).[148] Hereinto, doxorubicin was encapsulated with PEG-PCB for chemotherapy through strong hydrophobic and π–π interactions. Owing to a semiconducting backbone in PEG-PCB, DSPN5 could serve as a NIRF, PA imaging and photothermal agent. After systemic administration of DSPN5 in living mice, DSPN5 exhibited not only effective NIRF and PA imaging of tumors, but also superior antitumor efficacy over PEG-PCB or free DOX according to the synergistic effect of PTT and chemotherapy. In particular, Yang's group and Li's group, respectively, took advantage of SPNs with high photothermal conversion efficiency in combination with the antitumor drug for light-triggered drug release to enhance localized delivery, allowing for a synergistic therapeutic effect in a xenograft mouse model.[149–151] Additionally, a number of synergistic chemo-photothermal theranostic agents based on PPy were reported by Fan's group and Choi's group.[152,153] Our above study provides some evidence that it is feasible to develop imaging guided PTT and combined therapy of cancer with an excellent synergistic anti-tumor effect.

# 3. Photodynamic nanotherapeutics

NIR-absorbing organic nanoparticles not only could convert the absorbed light energy to produce heat for PTT, but also have the capability to induce ROS generation, thus allowing for PDT. Therefore, many NIR-absorbing organic nanoparticles have been reported to achieve highly promising results for PDT in several animal models. The $^1O_2$ quantum yield of NIR organic nanoagents is summarized and compared in Table 2 in the ESI.† For example, well-defined multicompartment micelles comprising polybutadiene-*block*-poly(1-methyl-2-vinyl pyridinium methyl sulfate)-*block*-poly(methacrylic acid) (BVqMAA) triblock copolymers and nanoparticles consisting of chlorin e6 (Ce6) and tumor-targeting RGD peptide modified poly (amido amine) (PAMAM) dendrimer were both used as advanced nanotheranostic agents for PDT.[154,155]

## 3.1. Imaging guided PDT

**3.1.1. Single-modal optical imaging guided PDT.** For the most common NIR organic nanoparticles, they can be employed as theranostic photosensitizers to image tumors conveniently before PDT for an enhanced therapeutic effect through different optical imaging methods, such as NIRF imaging,[156–163] aggregation-induced emission (AIE)[164] and positron emission tomography (PET).[165] For example, Zhang's group for the first time programmed a matrix metalloproteinase-2 (MMP-2) responsive ratiometric fluorescence biosensor for AIE-guided PDT.[164] Recently, organic nanotheranostic agents based on the widely used photosensitizer Ce6 have been mostly developed for NIRF imaging guided photodynamic treatment of tumors due to their NIR absorbance and high quantum yield of $^1O_2$.[156,166–168] Zhu and Yan's group used a two-photon absorption (2PA) hyperbranched conjugated polymer (HCP) and thermo-responsive hyperbranched polyether (HPE) to design a core–shell unimolecular micelle (HCP@HPE).[166] Then, Ce6 was grafted onto the surface of HCP@HPE for an enhanced cancer PDT because of the NIR-triggered fluorescence resonance energy transfer (FRET) process from the conjugated core to PSs, resulting from the collapsed thermo-responsive shell by the photothermal effect of NIR light. Additionally, hyaluronic acid nanoparticles (HANPs) were designed as the carrier of the hydrophobic photosensitizer Ce6 for simultaneous imaging and PDT.[156] And glutathione (GSH) activatable photosensitizer (PS)-conjugated pseudopolyrotaxane nanocarriers (α-CD-ss-Ce6 NPs) were reported for enhanced photodynamic theranostics.[167]

To enhance the therapeutic efficacy of PDT, some biocompatible and biodegradable self-assembled peptide and protein nanostructures have received comprehensive interest due to their ability to fulfil the specific demands of PDT using a controllable method. For instance, Yan *et al.* used short peptide-modulated self-assembly of photosensitizers to fabricate

 

nanotheranostic agents for enhanced photodynamic ablation of cancer.[168] In this study, Ce6 was self-assembled with both a diphenylalanine (H-Phe-Phe-$NH_2$·HCl, CDP) derived from FF and an amino acid derivative (9-fluorenylmethoxycarbonyl-L-lysine, Fmoc-L-Lys) to form the representative nanoparticles of Fmoc-L-Lys/Ce6 (FCNPs) and CDP/Ce6 (CCNPs) through several non-covalent interactions including π-stacking, electrostatic interactions and hydrophobic effects (Fig. 4a). They are responsive towards stimuli including pH, detergents and enzymes, which could facilitate selective release of photosensitizers in the tumor microenvironment. When incubated with MCF-7 cells under NIR laser irradiation, the photo-cytotoxicity of FCNPs and CCNPs measured by MTT was approximately 4-fold higher than that of the control group of free Ce6 (Fig. 4b). *In vivo* fluorescence images obtained at 24 h post-injection showed selective accumulation of FCNPs and CCNPs in tumors (Fig. 4c). Upon NIR laser irradiation, FCNPs showed superior PDT effects for enhanced tumor ablation compared to free Ce6 (Fig. 4d). The enhanced PDT efficacy *in vitro* and *in vivo* preliminarily indicated that this NP was a safe and excellent PDT organic nanoagent. Otherwise, this strategy provides the feasibility of a non-toxic drug delivery system for enhanced tumor phototherapy.

Some other NIR dyes, such as cyanine and protoporphyrin IX (PpIX), have also been utilized to fabricate organic nanotheranostic agents for NIRF imaging guided PDT of cancer.[157–159] Gao's group applied folate (FA) and heptamethine cyanine (Cy7)-modified chitosan (CF7) to self-assemble into nanoparticles (CF7Ns) for tumor-specific imaging and photodynamic therapy.[157] Similarly, protoporphyrin IX (PpIX) and PEG were conjugated with glycol chitosan (GC) to form GC-PEG-PpIX NPs, which could self-assemble into core–shell nanoparticles (NPs) for effective imaging-guided PDT.[158] For the first time, to effectively reduce self-quenching in nanocarriers at high concentrations, Hu and Wu's group developed a novel triple-effect PDT nanoagent with a special core–shell nanostructure by synergistic integration of perfluorotributylamine (PFTBA) and IR780 loaded HSA for improved PDT effects.[159]

Several NIR BODIPY derivatives were utilized to design photodynamic theranostic agents for NIRF imaging guided PDT through co-precipitation with an amphiphilic triblock copolymer.[160,161] For example, the novel photosensitizer BODIPY-Br2 and a galactose targeted amphiphilic copolymer of a polypeptide were co-precipitated to fabricate micelles for NIRF imaging-guided PDT of hepatoma cancer cells.[160] In another similar study, Han *et al.* synthesized a dual chromophore PS dyad (RET-BDP) comprising a distyryl-BODIPY moiety (B-1) as the donor and fluorophore, and a diiodo-distyryl-BODIPY moiety (B-2) as the acceptor and PS.[161] Then, RET-BDP was encapsulated by F-127-FA to form the folic acid conjugated nanomicelles (RET-BDP-TNM) for efficient PDT *in vitro* and *in vivo* under low-power LED light irradiation (Fig. 5a). The broader and stronger absorption spectra of RET-BDP triggered a higher $^1O_2$ quantum yield, which was improved by 1.9- and 1.6-fold compared to the photosensitizer B-2 and the widely used photosensitizer Ce6. Thus, $^1O_2$ generation of RET-BDP-TNM was measured and quantified, which was amplified by 1.8-fold relative to that of B2-TNM alone using the $^1O_2$ scavenger 1,3-diphenylisobenzofuran (DPBF) (Fig. 5b). The phototoxicity of B1-TNM, B2-TNM, and RET-BDP-TNM was measured by MTT assays, showing the

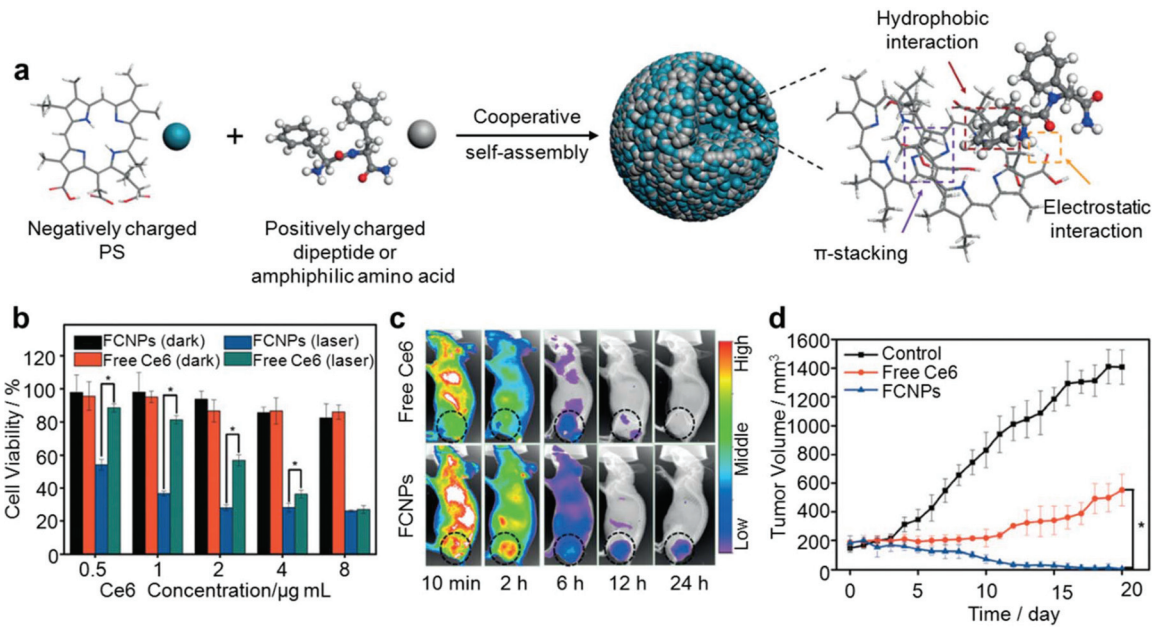


**Fig. 4** Amphiphilic dipeptide- or amino-acid-tuned self-assembly of photosensitizers for PDT. (a) A schematic illustration of the self-assembly process. (b) *In vitro* cytotoxicity and photocytotoxicity of FCNPs. (c) Fluorescence images of FCNPs and free Ce6 treated tumor-bearing mice. (d) Tumor growth curves of the mice after injecting FCNPs and free Ce6. Reproduced from ref. 168 with permission from WILEY-VCH.

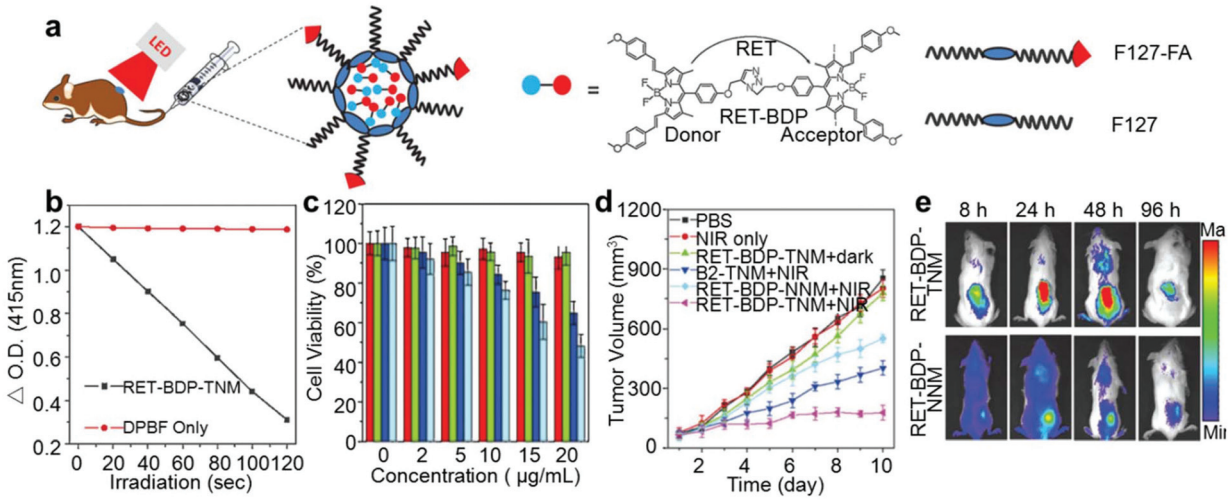


**Fig. 5** RET-photosensitizer nanomicelles (RET-BDP-TNM) for NIRF and guided PDT. (a) A schematic illustration for PDT of RET-BDP-TNM and the molecular structure of RET-BDP. (b) $^1O_2$ generation of RET-BDP-TNM under NIR light irradiation (10 mW cm$^{-2}$). (c) Relative viability and photocytotoxicity of 4T1 cells incubated with different concentrations of RET-BDP-TNM and B2-TNM. (d) Changes in tumor sizes in different groups after treatment. (e) *In vivo* NIRF images of 4T1 tumor-bearing mice after intravenous injection of RET-BDP-TNM and RET-BDP-NNM. Reproduced from ref. 161 with permission from WILEY-VCH.

superior PDT effect of RET-BDP-TNM relative to B2-TNM (Fig. 5c). *In vivo* NIRF imaging was performed on BALB/c mice with 4T1 breast tumors after intravenous injection of RET-BDP-TNM (Fig. 5e). The fluorescence intensity of the tumor treated with RET-BDP-TNM was found to be significantly enhanced after 8 h, and reached a maximum after 24 h. Meanwhile, the fluorescence was higher than that of folic-acid-free nanomicelles (RET-BDP-NNM), suggesting that the folic acid ligand contributed to the accumulation of RET-BDP-TNM at the tumor site. Additionally, RET-BDPTNM could be activated by low-power NIR LED sources, which led to efficient tumor inhibition *in vivo*, indicating RET-BDPTNM as a superior NIR-absorbing organic PDT nanotheranostic agent (Fig. 5d). This work demonstrates the promise of those NIR dye based nanoparticles in imaging-guided PDT of cancer.

Novel NIR-absorbing SPNs have emerged as a new class of photonic nanotheranostic agents for NIFR imaging guided PDT.[162,163] Wang *et al.* programmed multimodal polymer nanoparticles (PNPs) based on polythiophene derivatives for two-photon fluorescence imaging and two-photon-excited PDT.[162] This designed multifunctional PNP could be a promising PDT nanoagent owing to simultaneous cellular, deep-tissue imaging, and highly efficient *in vivo* PDT for cancer. Li *et al.* just applied a photosensitizer (PS) and small interfering RNA (siRNA) to design a micelleplex for enhanced cancer PDT by immunotherapy.[169] Recently, our group also designed SPN-based nanotheranostics with self-regulated NIR photodynamic properties for optimized cancer therapy.[163] In this system, the nanotheranostic agent was composed of a NIR-absorbing SP as the NIR fluorescent PDT agent and a nanoceria as the smart intraparticle regulator to act as a ROS scavenger and converter in a physiologically neutral and pathologically acidic environment (Fig. 6a). When exposed to NIR laser irradiation, ROS generation for SPNs under both physiologically neutral (pH = 7.4) and pathologically acidic (pH = 6.5) conditions was, respectively, monitored and quantified by 2′,7′-dichlorofluorescin diacetate ($H_2$DCFDA), $^1O_2$ sensor green (SOSG), and Amplex Red, verifying that doping of nanoceria into SPNs (SPN-C23) could enhance the ROS production under acidic conditions but reduce the ROS production under neutral conditions since superoxide was converted into hydrogen peroxide and oxygen, respectively, under these conditions (Fig. 6b–d). The PDT efficacy of SPNs *in vitro* was studied using a 4T1 mouse mammary tumor cell line (Fig. 6e). Under 808 nm laser irradiation (0.44 W cm$^{-2}$), cell ablation for SPN-C23 was 2.9-fold higher than that for SPN without doping nanoceria (SPN-0) at 25 μg mL$^{-1}$. In contrast, both SPNs showed no cytotoxicity at a concentration up to 25 μg mL$^{-1}$. After intravenous injection of SPNs, the NIR fluorescence images were obtained and quantified using a xenograft 4T1 tumor mouse model, showing that the fluorescence intensity at the tumor site for both SPNs reached the maximum at 6 h post-injection (Fig. 6g). Additionally, as confirmed by the photodynamic effect of intramuscular nanoparticles in living mice, the nanoceria doping of SPN-C23 facilitated enhanced PDT efficiency and minimized damage to normal tissue during the PDT process (Fig. 6f). Additionally, our group recently developed hybrid core–shell SPN-based nanotheranostic agents (SPN-Ms) for promoted PDT through $O_2$ generation in hypoxic solid tumors from the reaction of $MnO_2$ nanosheets and hydrogen peroxide ($H_2O_2$).[15] Therefore, as many inorganic nanocomposites can be inserted into SPNs, a variety of hybrid optical nanotheranostic agents based on SPNs may be developed for *in vivo* imaging and enhanced PDT of tumors.

**3.1.2. Multimodal imaging guided PDT.** In addition to single-modal NIRF imaging guided PDT, dual- and triple-

 

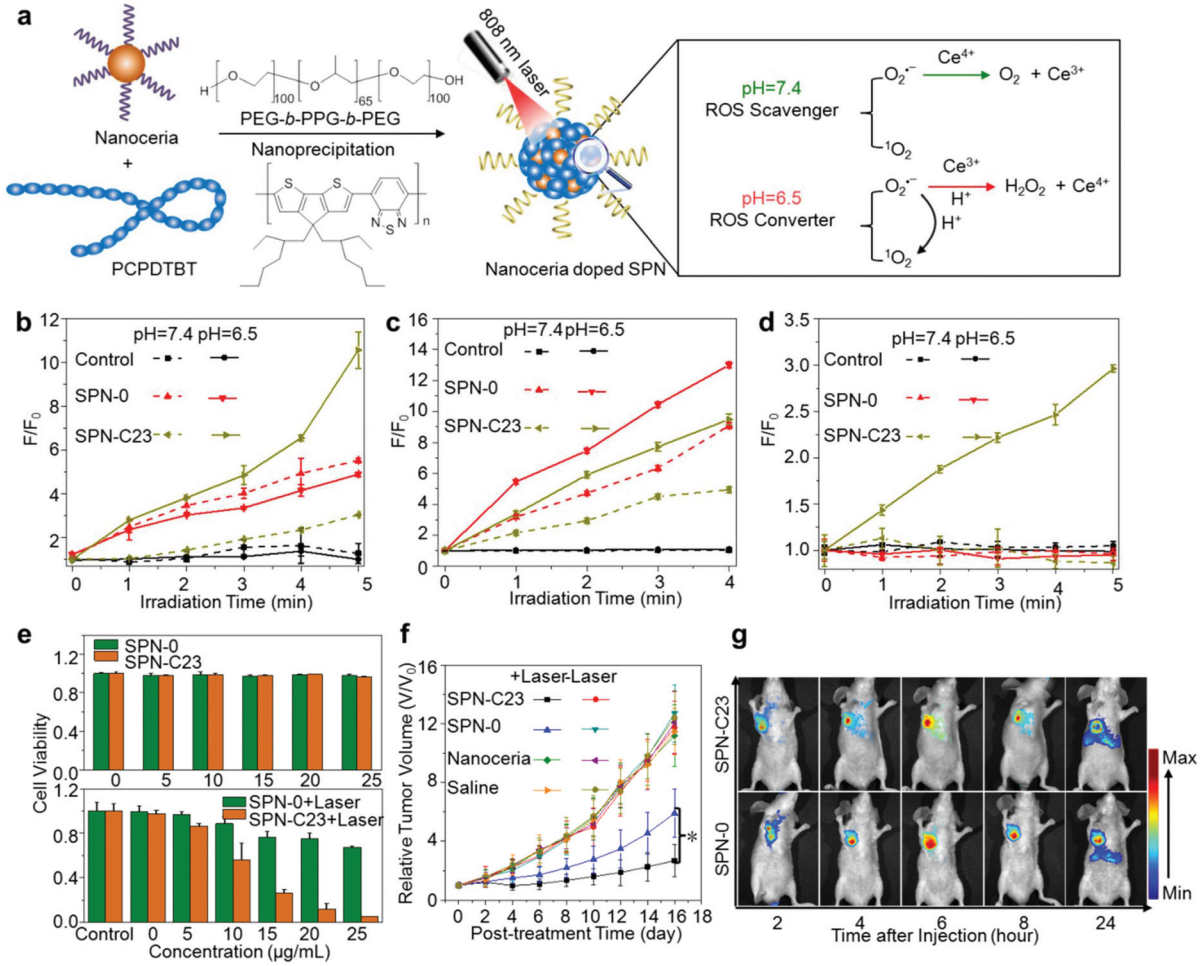


**Fig. 6** Nanoceria-doped SPNs for NIRF imaging-guided PDT. (a) A schematic illustration of synthesizing nanoceria-doped SPNs and the mechanism of photodynamic properties of SPNs at different pH values. (b) Total ROS, (c) $^1O_2$, and (d) hydrogen peroxide generation from SPNs under NIR laser irradiation (0.44 W cm$^{-2}$). (e) *In vitro* cytotoxicity and photocytotoxicity of SPNs. (f) Tumor growth curves of mice after different treatments. (g) Fluorescence images of a 4T1 xenograft tumor after systemic administration of saline or SPNs. Reproduced from ref. 163 with permission from American Chemical Society.

modal imaging guided PDT nanoagents based on NIR organic nanoparticles have been developed to overcome the limitations of each single imaging modal. Hereinto, PA-integrated NIRF imaging was a classic dual-modal imaging strategy with high temporal and spatial resolution. NIRF/PA dual-modal imaging guided PDT has been investigated in several animal model experiments.[170] Cai *et al.* reported smart hyaluronidase-activated nanotheranostic agents for NIRF/PA imaging guided PDT.[170] In this nanoagent, the NIR dye (Ce6) was firstly used to conjugate with hyaluronic acid (HA) with three different molecular weights to form the conjugates utilizing adipic dihydrazide (ADH) as linkages (HA–ADH–Ce6), which then self-assembled into HACE nanoparticles in water. When irradiated with a NIR laser, the fluorescence intensity and PA signal in the tumor bearing mice treated with HACE NPs were 5 and 3-fold higher than those of free Ce6, respectively.

Besides the NIRF/PA dual-modal imaging guided PDT, NIR absorbing organic nanoparticles have also been employed for NIRF/MR imaging guided PDT, combining the sensitivity of the former and the high spatial and temporal resolution of the latter.[171,172] Tan *et al.* recently designed a multifunctional nanostructure (ICG-FA-PPD) self-assembled by ICG and folic acid (FA) modified poly(ethyleneimine) (PEI)-PEG-gadoteric acid (Gd-DOTA) (FA-PPD) for photodynamic ablation of cancer guided by synchronous NIRF/MR imaging.[172] Accordingly, a theranostic platform (HAGCP-NPs), which was constructed through the encapsulation of Ce6 into poly(lactic-*co*-glycolic acid) nanoparticles coated with HA and then chelation of $Gd^{3+}$, has been developed for the dual-modal (NIRF/MR) imaging and PDT of cancer.[171]

Additionally, other dual-modal imaging guided PDTs have also been developed for NIR-absorbing organic nanomaterials. For instance, an organic PDT system (PEG-Ce6 nanomicelles) guided by NIRF and PET imaging was simply constructed through the conjugation of PEG-coated nanomicelles with Ce6, which was then chelated with $^{64}Cu$ for *in vivo* PET.[165] Thus, these investigations further indicated the potential of NIR organic nanoparticle-based multifunctional nanotheranostics in multimodal imaging guided PDT of cancer.

### 3.2. Chemo-photodynamic nanotherapeutics

In the recent years, the combination of chemotherapy with PDT has been extensively applied in both preclinical research and clinical tumor treatment. This was mainly due to the mutual promotion interaction between chemotherapy and PDT, including suppression of the over-expressed active efflux translocator and inhibition of the drug-efflux probability by $^1O_2$ or other ROS from PDT, as well as improved tumor sensitivity to PDT by chemotherapeutic effects. Taratula *et al.* designed a phthalocyanine based theranostic agent (Pc-LHRH) for chemo-photodynamic therapy of tumors through the initial encapsulation of monosubstituted phthalocyanine (PcSi-(OH)(mob)) into a PPI dendrimer followed by the modification of the dendrimer surface with PEG and a luteinizing hormone-releasing hormone (LHRH) peptide.[173] Furthermore, hydrazone-based pH-sensitive polymeric micelles entrapped by the novel NIR-BODIPY photosensitizer were designed and loaded with DOX for NIRF imaging-guided chemo-photodynamic cancer therapy.[174]

SPN-based chemo-photodynamic nanotheranostic agents have also been reported. Liu's group recently fabricated a novel theranostic platform comprising a conjugated-polyelectrolyte (CPE) polyprodrug for imaging guided chemo-photodynamic therapy.[175] In this system, the PEGylated CPE as the PS and carrier was covalently conjugated to DOX through a linker, which could be cleaved by ROS. Thus, when irradiated with appropriate light, the ROS generated from CPE could be used not only for PDT, but also for on-demand drug release and chemotherapy, leading to enhanced therapeutic efficiency.

PDT was known to be a noninvasive cancer therapeutic method triggered by light, consequently leading to severe tumor hypoxia. Therefore, several hypoxia-activated prodrugs, including 4-[3-(2-nitro-1-imidazolyl)-propylamino]-7-chloroquinoline hydrochloride (NLCQ-1), banoxantrone (AQ4N), tirapazamine (TPZ) and dinitrobenzamide mustards, which could be activated in an oxygen-deficient environment,[176,177] have been widely developed to potentiate the antitumor efficacy of PDT.[177–179] Recently, a cancer cell membrane-coated nanoplatform based on the TPZ-loaded porphyrinic metal organic framework (TPZ@PCN@Mem) was designed for tumor-targeting PDT, successively resulting in hypoxia amplified bioreductive therapy.[178] Similarly, Oupicky and Zhou's group developed hybrid PLGA/lipid nanoparticles for fluorescence imaging and chemo-photodynamic therapy of metastatic breast cancer due to co-delivery of a photosensitizer (ICG) and the hypoxia-activated prodrug TPZ (NP/IT).[179] To possess the intratumoral penetration capability and improved antitumor performance, the nanoparticles were further conjugated with iRGD through copper-free click chemistry (Fig. 7a). In this study, ICG acted as a ROS generator and oxygen consumer upon NIR laser irradiation under normal oxygen conditions, consequently inducing the hypoxic microenvironment in tumors that could trigger TPZ to enhance local cell killing (Fig. 7b). The ability of iNP/IT to generate ROS was validated using DPBF, a $^1O_2$ probe, upon NIR laser irradiation (Fig. 7c). The excellent combined cancer cell killing effect of the co-delivered photosensitizer and chemotherapeutic drug was determined by measuring the viability of the 4T1 cells treated with different drug formulations with or without laser irradiation under normoxic con-

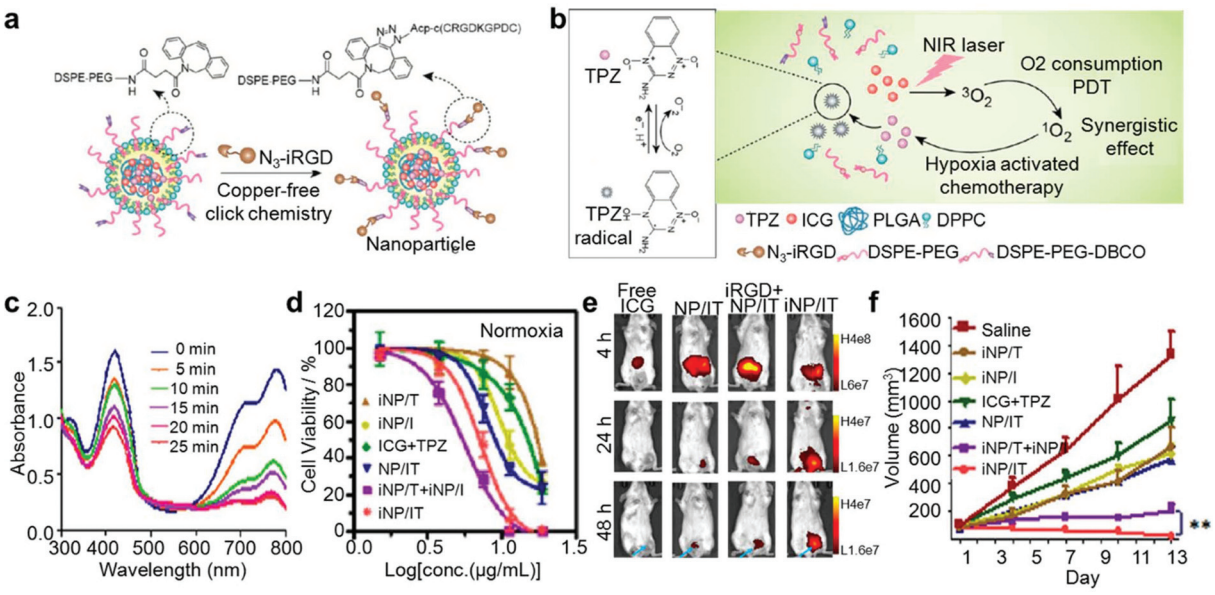


Fig. 7 iRGD modified nanoparticles loaded with ICG and TPZ (iNP/IT) for the combined PDT and hypoxia-activated treatment of tumors. (a) A schematic illustration of the preparation of iNP/IT nanoparticles. (b) A scheme showing the synergistic photodynamic and hypoxia-activated therapeutics of iNP/IT nanoparticles. (c) $^1O_2$ generation of iNP/IT nanoparticles under 808 nm laser irradiation (2 W cm$^{-2}$). (d) *In vitro* cytotoxicity and photocytotoxicity of iNP/IT under normoxic conditions. (e) *In vivo* fluorescence images of tumor-bearing mice after intravenous injection of free ICG and different nanoparticles. (f) Tumor growth curves in mice after different treatments. Reproduced from ref. 179 with permission from American Chemical Society.

 

ditions (Fig. 7d). The capacity of iRGD modified iNP/IT for improved delivery and penetration in solid tumors *in vivo* was evaluated through comparing the fluorescence imaging performance of iRGD modified iNP/IT on mice bearing orthotopic 4T1 tumors (Fig. 7e). The combination therapy using the tumor-penetrating nanoparticle was evaluated in a metastatic orthotopic 4T1 mammary adenocarcinoma model (Fig. 7f). Upon NIR laser irradiation, the strongest antitumor effect with iNP/IT was observed as compared to all the controls including iRGD-targeted nanoparticles loaded with a single drug (iNP/I and iNP/T) and a combination of free drugs (ICG + TPZ), as well as in mice treated with nonpenetrating nanoparticles (NP/IT), indicating the excellent synergistic effect of the ICG-mediated PDT and the hypoxia-activated TPZ chemotherapy. Thus, these NIR organic nanoparticles presented an effective strategy for enhanced anticancer therapy.

Additionally, Liu *et al.* developed a liposome-based nanotheranostic agent with a sequential activation pattern for PA, NIRF, and PET imaging guided PDT-induced hypoxia-activated cancer therapy.[177] This nanotheranostic agent was fabricated through the respective encapsulation of hydrophilic AQ4N and hydrophobic hexadecylamine conjugated Ce6 into the aqueous cavity and hydrophobic bilayer of PEG shelled liposomes and the following chelation of the $^{64}$Cu isotope for PET imaging. In this system, upon 660 nm light-emitting diode light, the photodynamic effect would induce severe tumor hypoxia, in turn triggering activation of AQ4N. Consequently, this sequential PDT and hypoxia activated chemotherapy of the nanotheranostic agent would remarkably enhance cancer therapy efficacy compared to conventional cancer PDT. These examples showed that NIR organic nanoparticles could be developed into effective nanotheranostics for the combined drug delivery and imaging guided tumor PDT with enhanced efficacy.

# 4. Combined photothermal/photodynamic nanotherapeutics

PTT and PDT are known to be the two main noninvasive medical techniques in treating various diseases including tumor. The combination of PTT and PDT not only triggered the photothermally enhanced PDT efficiency, but also induced a synergistic effect – the photothermal effects can accelerate intratumoral blood flow, thus leading to more oxygen transported into tumor to amplify the PDT efficacy.[15,180–182] To compare PDT and PTT efficacy of porphysomes in hyperoxic and hypoxic tumors, for the first time, Zheng's group investigated the nanostructure-driven conversion of the mechanism of PDT activation of porphyrin to PTT activation in an *in vivo* hypoxic tumor model.[183] Additionally, a platinated boron dipyrromethene (BDP) core (Bodiplatin-NPs) and silicon naphthalocyanine based phototheranostics were, respectively, designed for photoinduced cancer therapy of tumor ablation.[184,185] Also, Zhou *et al.* and Kim *et al.*, respectively, combined NIR dyes-ICG and -IR780 with SPs-PEDOT and -PPy to fabricate novel synergistic agents in combined PTT and PDT to inactivate pathogenic bacteria and treat tumors.[186,187]

## 4.1. Imaging guided photothermal/photodynamic nanotherapeutics

**4.1.1. Single-modal optical imaging guided PDT/PTT.** Commonly, several NIR dyes including Ce6,[188,189] ICG,[190,191] IR780[192,193] and silicon naphthalocyanine[194] have been developed to be nanotheranostic agents for simultaneous synergistic PTT/PDT guided by NIRF imaging. In addition, SPs with high NIR absorbance based nanoagents also showed potential applications for NIRF imaging guided synergistic PTT/PDT. Liu and Ding's group synthesized two SPs, poly[9,9-bis(2-(2-(2-methoxyethoxy)-ethoxy)-ethyl)fluorenyldivinylene]-*alt*-4,7-(2,1,3-benzothiadiazole) as a NIR fluorescent photodynamic agent, and poly[(4,4,9,9-tetrakis(4-(octyloxy)-phenyl)-4,9-dihydro-*s*-indacenol-dithiophene-2,7-diyl)-*alt-co*-4,9-bis(thiophen-2-yl)-6,7-bis(4 (hexyloxy)phenyl)-thiadiazolo-quinoxaline] as a photothermal agent to co-load into one single SPN *via* an encapsulation approach using lipid-PEG as the matrix.[195] With a high $^1O_2$ quantum yield of 60.4% and an effective photothermal conversion efficiency of 47.6%, the obtained SPNs modified with anti-HER2 affibody not only endowed superior selectivity toward tumor cells with HER2 overexpression both *in vitro* and *in vivo*, but also possessed synergistic therapeutic efficacy of PTT/PDT for cancer treatment.

Because of the close relation between the PA signal and photothermal conversion, PA imaging guided phototheranostics with the synergistic effect of PTT/PDT have also been designed. In Dong's group, they synthesized a pH-sensitive photosensitizer (NAB) through introducing a pH-sensitive receptor (dimethylaminophenyl unit) onto the aza-BODIPY core and a BF2 chelate of [4-iodo-5-(4-bromophenyl)-3-(4-methoxyphenyl)-1*H*-pyrrol-2-yl][4-iodo-5-(4-bromophenyl)-3-(4-methoxyphenyl)pyrrol-2-ylidene]amine (IABDP) with high $^1O_2$ generation efficiency (92%) and high photothermal conversion efficiency (37.9%) to fabricate NIR-absorbing organic nanotheranostic agents for PA imaging guided simultaneous PTT and PDT.[196,197] At the same time, they designed a donor–acceptor–donor (D–A–D) structured small molecule (DPP-TPA) to self-assemble into a single component DPP-based organic nanotheranostic agent (DPP-TPA NPs) for PA imaging-guided PTT/PDT (Fig. 8a).[198] In this agent, the thiophene group of the diketopyrrolopyrrole (DPP) molecule could enhance the intersystem crossing (ISC) ability through the heavy atom effect. Simultaneously, triphenylamine (TPA) with bathochromic shift absorption and charge transport capacity enhancement as a typical donor was conjugated with the DPP core to form a NIR-absorbing D–A–D molecule. After the formation of a nanoparticle architecture, the capacity of charge transport and heat generation was greatly impelled, inducing the DPP-TPA NPs to have a high photothermal conversion efficiency of 34.5%, as well as an excellent $^1O_2$ quantum yield of 33.6% under NIR laser irradiation (Fig. 8b & c). Cytotoxicity and photocytotoxicity of HeLa cells incubated with DPP-TPA NPs with various concentrations were evaluated using an MTT assay under

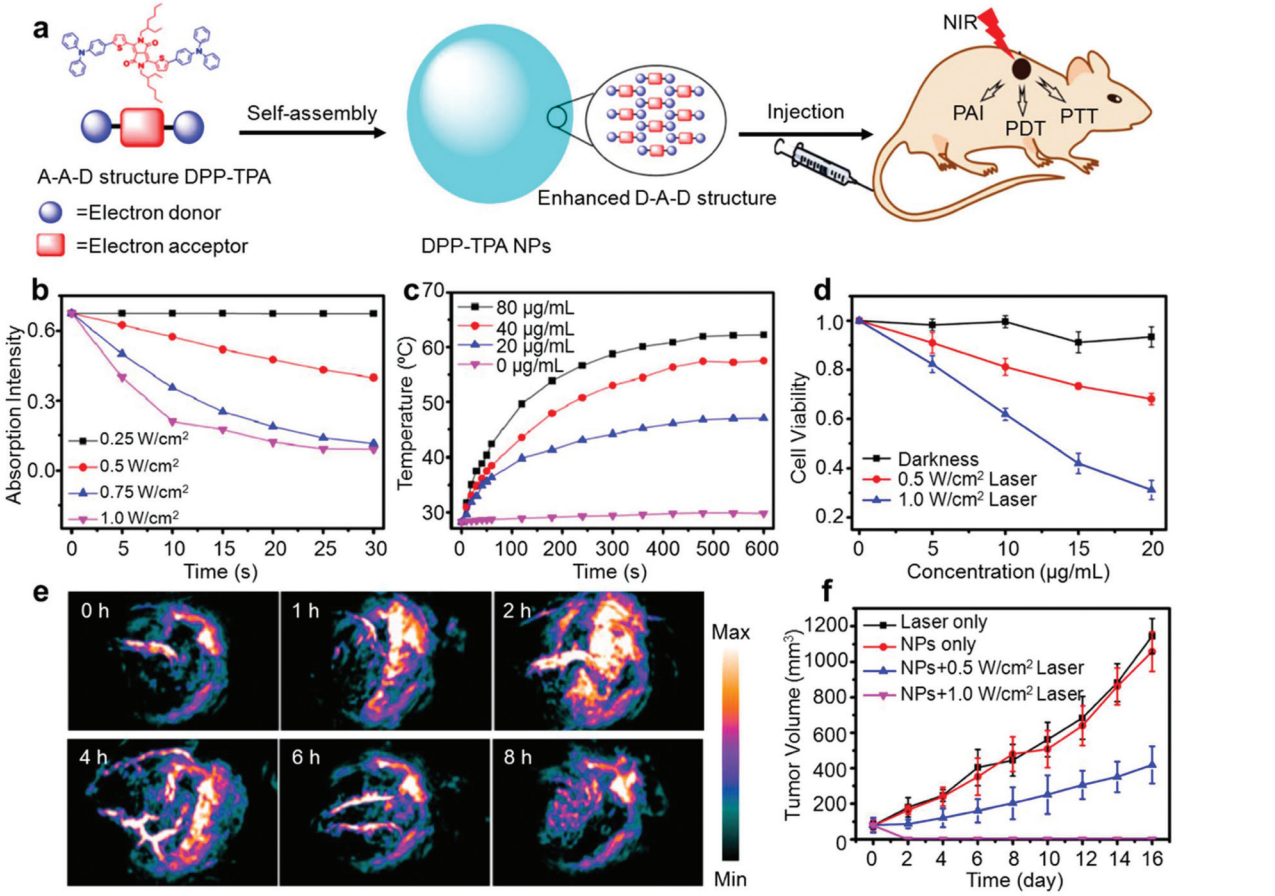


**Fig. 8** Enhanced D–A–D structured DPP-TPA NPs for PA imaging guided synergistic PTT and PDT. (a) A scheme illustrating the synthesis of D–A–D structured DPP-TPA NPs and their PA imaging guided PTT/PDT. (b) $^1O_2$ production of DPP-TPA NPs under NIR laser irradiation. (c) Temperature curves of DPP-TPA NPs under NIR laser irradiation (1 W cm$^{-2}$). (d) Cytotoxicity and photocytotoxicity of HeLa cells incubated with various concentrations of DPP-TPA NPs. (e) PA images in tumor sites after intravenous injection of DPP-TPA. (f) Changes in tumor volumes in various treatment groups. Reproduced from ref. 198 with permission from American Chemical Society.

different irradiating conditions, demonstrating the efficient synergistic photodynamic/photothermal efficiency of DPP-TPA NPs (Fig. 8d). As confirmed by real-time *in vivo* PA images of a tumor site after intravenous injection of DPP-TPA NPs into mice, DPP-TPA NPs possessed excellent ability of PA imaging and tumor targeting *in vivo* (Fig. 8e). Furthermore, the tumor growth curves depicted that the tumor injected with DPP-TPA NPs could be inhibited under NIR laser irradiation with both lower and higher power density, and the tumors under higher power irradiation were totally eliminated in the first treatment owing to larger temperature increment and more ROS generation (Fig. 8f). These results further demonstrated the excellent synergetic PA imaging guided PTT/PDT of DPP-TPA NPs *in vivo*. Thus, the synchronous combination of PDT with chemotherapy proved to have a synergistic and excellent therapeutic efficiency compared to single modality treatment.

**4.1.2. Multimodal imaging guided PTT/PDT.** Based on PA imaging, multimodal imaging combined with other imaging techniques including NIRF and MR imaging has been utilized to guide simultaneous PTT/PDT. For instance, Chen *et al.* loaded the widely used photosensitizer (Ce6) into a micelle-encapsulated cyanine dye, realizing simultaneously synergistic PTT/PDT guided by dual-modal NIRF and PA imaging.[199] Cai and Ma's group applied ICG assembled with an endogenous HSA programmed multifunctional nanotheranostic system and applied it for tumor margin detection and synergistic PTT/PDT combined with dual-modal NIRF and PA imaging.[200] This HSA-ICG nanoparticle was obtained by using GSH to cleave the disulfide bonds of HSA molecules to form HSA with free sulfhydryl groups, which were then assembled again with ICG by intermolecular disulfides. Under NIR laser irradiation, this HSA-ICG nanoparticle showed excellent fluorescence and PA imaging properties, as well as superior PDT for tumors. In another study, a hexylamine conjugated Ce6 (hCe6) dye and a lipophilic NIR dye, 1,1′-dioctadecyl-3,3,30,3′-tetramethylindotricarbocyanine iodide (DiR), were applied to synthesize PEG shelled liposomes (DiR-hCe6-liposome) for NIRF and PA imaging guided synergistic PTT/PDT.[201] In the prepared nanoparticles, FRET occurred between hCe6 and DiR, quenching the fluorescence and photosensitizing effect of hCe6.

 

Additionally, irradiation with a 785 nm NIR laser induced the photobleaching of DiR, conversely activating both the fluorescence and photodynamic effect of hCe6 in DiR-hCe6-liposome (Fig. 9a). The ability of DiR-hCe6-liposome to generate $^1O_2$ could be verified as it could only produce ~18% and ~16% of $^1O_2$ compared to that of hCe6-liposome and free Ce6 under only 660 nm laser irradiation, but it could generate ~90% and ~77% of $^1O_2$ under combined laser irradiation at 785 and 660 nm (Fig. 9b). Afterwards, the NIR-activated PDT effects of DiR-hCe6-liposome were also evaluated at the cellular level through the standard cell viability assay (Fig. 9c). Meanwhile, under such NIR irradiation, tumors of DiRhCe6-liposome injected mice were mildly heated (Fig. 9d), in turn amplifying the intra-tumor blood flow and reliving tumor hypoxia, which consequently contributed to the enhanced photodynamic tumor treatment. Considering the strong NIR absorbance and fluorescence of DiR, NIRF and PA imaging of the tumor treated with DiR-hCe6-liposome was conducted, and the gradually increased fluorescence and PA signals in the tumor were observed following the injection of DiR-hCe6-liposome (Fig. 9e & f). Under the guidance of simultaneous NIRF and PA imaging, DiR-hCe6-liposome showed an excellent tumor ablation capability through NIR light-activated PDT over conventional PDT (Fig. 9g). All these results highlighted that this is a meaningful strategy to design new generation of NIR organic nanotheranostics with multimodal imaging and combined therapy for cancer.

Besides this, a donor–acceptor (D–A) structured polymer (TBT) based nanotheranostic agent, which possessed an excellent $^1O_2$ quantum yield (40%) and high photothermal conversion efficiency (37.1%) under NIR laser irradiation (635 nm), was developed for NIRF/PA/thermal imaging guided PTT/PDT.[202] Recently, an NIR dye-conjugated hydroxyl radical generating biodegradable polymer (HRGP-IR) was designed to self-assemble to form theranostic micelles with elevated oxidative stress by producing hydrogen peroxide and hydroxyl radical.[203]

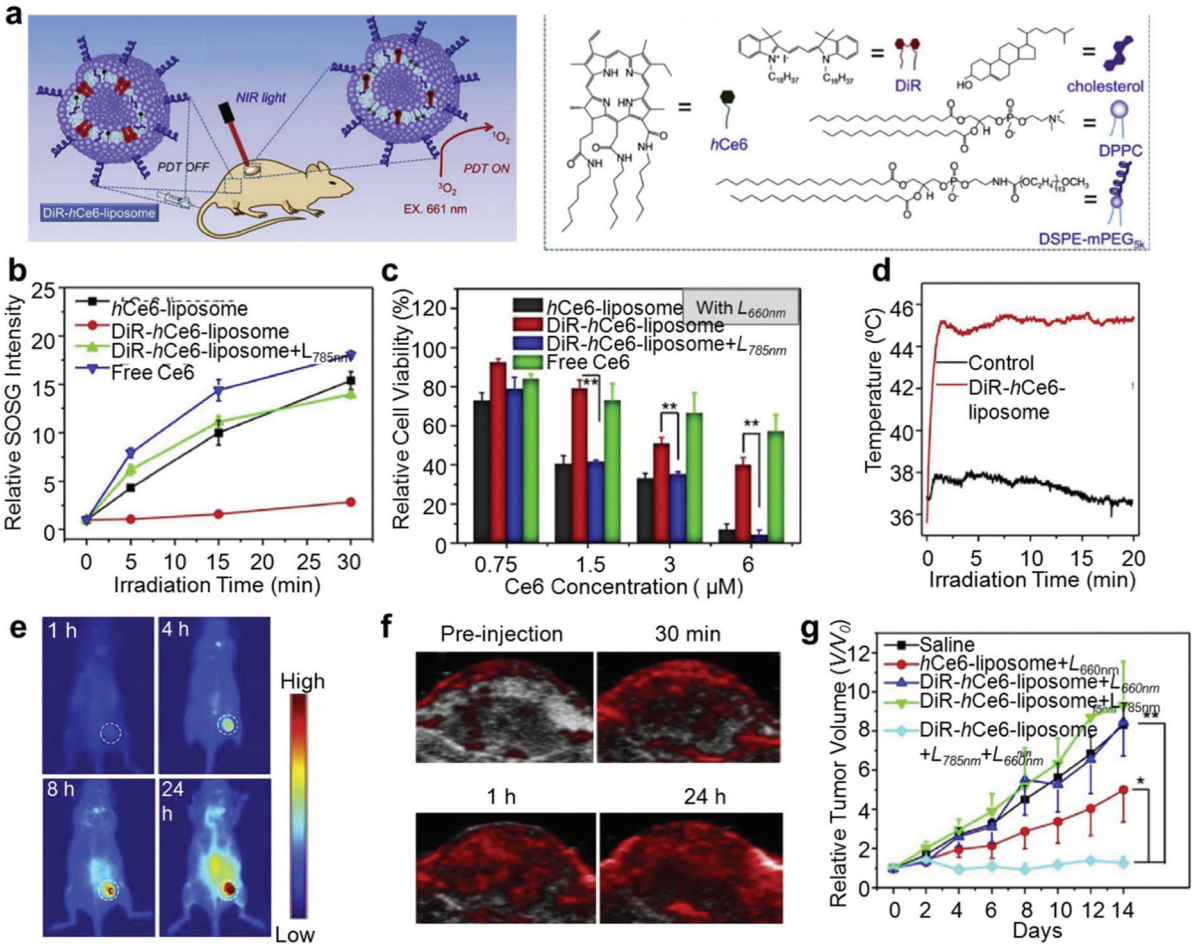


**Fig. 9** DiR-hCe6-liposome for PA imaging guided synergistic PTT and PDT. (a) A schematic illustration of the synergistic cancer phototherapy of DiR-hCe6-liposome and chemical structures of these molecules. (b) $^1O_2$ generation of DiR-hCe6-liposome, hCe6-liposome, and free Ce6 with and without 785 nm laser irradiation. (c) Relative viabilities and photocytotoxicity of 4T1 cells incubated with hCe6-liposome, DiR-hCe6-liposome, and free Ce6. (d) A temperature curve of DiR-hCe6-liposome under 785 nm laser irradiation (0.7 W cm$^{-2}$). (e) *In vivo* fluorescence images and (f) PA images of 4T1 tumor-bearing mice after intravenous injection of DiR-hCe6-liposome. (g) Tumor growth curves of mice after various different treatments as indicated for 14 days. Reproduced from ref. 201 with permission from Elsevier Ltd.

When irradiated with an 808 nm laser, HRGP-IR micelles showed highly potent synergistic anticancer activity of combined PTT/PDT after giving dual-modal NIRF and PA imaging.

Synergistic photodynamic/photothermal nanotheranostics with NIRF, PA imaging and MR imaging properties were also reported. For instance, Liu's group simply combined PPy with Ce6 conjugated BSA and labeled Gd to the fabricated nanotheranostic agent (PPy@BSA-Ce6) for dual-modal NIR and MR imaging guided photothermal and photodynamic treatment of tumors.[204] Also, a multifunctional lipid-micelle (Pdots/Ce6@lipid–Gd–DOTA micelles), which comprised semiconducting polymer dots (Pdots), a photosensitizer (Ce6) and a lipid–PEG outlayer conjugated with gadolinium-1,4,7,10-tetraacetic acid, was designed for combined MR/PA imaging and PTT/PDT.[205] In another study,[206] an amphiphilic poly [(poly(ethylene glycol)methyl ether methacrylate)-*co*-(3-aminopropyl methacrylate)]-*block*-poly(methyl methacrylate) (P(PEGMA-*co*-APMA)-*b*-PMMA) block copolymer was synthesized to self-assemble with 5,10,15,20-tetrakis(4-carboxyphenyl)porphyrin (TCPP) labeled with $Mn^{2+}$ as a tetra-functional cross-linker, a photodynamic agent, a fluorescence indicator, and a MR contrast agent, as well as a NIR dye (IR825) as a photothermal agent and PA agents to form a nanotheranostic agent (IR825@P(PEGMA-*co*-APMA)-*b*-PMMA@TCPP/Mn). Liu's group recently fabricated two kinds of nanotheranostic agents based on sinoporphyrin sodium (DVDMS) as a photosensitizer for NIRF/PA and/or MR imaging guided phototherapy of cancer: (i) $MnO_2$ nanosheets as a DVDMS carrier and an *in situ* oxygen generator to activate imaging signals and improve PDT efficacy, and (ii) RGD-modified ferritin (R-Fn) nanocages to highly efficiently load DVDMS.[180,207] These nanoagents were successfully applied for triple-modal imaging guided PTT/PDT of tumors. Similarly, one nanotheranostic agent composed of Ce6, the NIR dye IR825 and a chelating agent for $Gd^{3+}$ and another nanoplatform with chelating $Gd^{3+}$ and Ce6 in PPy using BSA as the stabilizing agent were, respectively, developed for triple modal NIRF/MR/PA and dual-modal NIRF/MR imaging guided phototherapy of tumors in a mouse model.[208,209] These nanotheranostics presented great potential in both multimodal imaging and combined therapy of tumors.

### 4.2. Chemo/photodynamic/photothermal nanotherapeutics

Although the combination of PTT and PDT has been reported to enhance therapeutic efficiencies, certain limitations still exist, including survival of the residual cells after photothermal injury and the hypoxia microenvironment induced by PDT. Therefore, combining phototherapy with chemotherapy was also thought to be an alternative approach for further improving therapeutic efficacy. Liu's group used poly(2,3-dihydrothieno-1,4-dioxin)-poly(styrenesulfonate) (PEDOT:PSS) nanoparticles coated with PEG to develop organic nanotheranostic agents with triple-modal therapy, in which drugs (DOX or SN38) and the photodynamic agent Ce6 through π–π stacking and hydrophobic interactions were loaded.[210] In these as-prepared nanoparticles, not only the loading of Ce6 on PEDOT:PSS-PEG could accelerate cellular uptake, but also the photothermal effect of PEDOT:PSS-PEG could promote drug delivery, enabling combined photodynamic, photothermal and chemotherapy for synergistic cancer cell killing. In a similar way, docetaxel (DTX) loaded micellar nanomedicines co-loaded with the NIR dye-IR820 and poly(vinyl alcohol)-porphyrin based nanotheranostic agents (PPNs) loaded with DOX were respectively constructed for PDT/PTT/chemotherapy of cancer.[211,212] Additionally, to combat drug resistance of cancer cells, an ultra-pH-responsive diblock copolymer, poly(ethylene glycol)-*block*-poly(diisopropanol amino ethyl methacrylate cohydroxyl methacrylate) (PDPA), was used to construct intracellularly acid-switchable multifunctional micelles for PDT/PTT/chemotherapy of the drug-resistant tumor.[213] In this system, the micelles were mainly composed of a pH-responsive diblock copolymer (PDPA) as the acid-responsive matrix, a photosensitizer (Ce6) chelated by $Gd^{3+}$ as the PDT, NIRF and MR imaging agent, and a polymeric prodrug of doxorubicin (PDOX) as the chemotherapy agent. When irradiated with a NIR laser, the micelles could not only produce ROS to trigger PDOX release for NIRF and MR imaging guided chemo-photodynamic therapy, but also generate heat for enhancing tumor penetration of the anticancer drug and realizing PA imaging guided PTT. Therefore, the micelles exhibited good potential for combinational PDT/PTT/chemotherapy of drug-resistant tumors with the guidance of triple-modal NIRF, MR, and PA tumor imaging.

## 5. Conclusion and perspective

This review mainly describes the recent progress on NIR-absorbing organic nanoparticles for cancer phototherapy with the emphasis on different modal imaging guidance. With many unique properties, including highly efficient light harvesting and emitting features, good cytocompatibility, and versatile surface modification, NIR-absorbing organic nanoparticles can not only serve as versatile optical nanoagents for NIRF, chemiluminescence and PA imaging, but also act as phototherapeutic agents for cancer therapy. The labeling of MR, US and CT contrast or loading of drugs into NIR-absorbing organic nanoparticles endow them with multifunctional properties for single modal or multimodal imaging guided phototherapy and photo-chemotherapy.

However, despite the recent exciting outcomes from NIR-absorbing organic nanomaterials for phototherapies, there are still several issues remained to be addressed before their future clinical translation, including (i) the low photostability of some NIR dyes inducing low efficiency of heat generation, (ii) the relatively poor ability to generate $^1O_2$ despite high NIR absorbance, (iii) long-term biodegradability and clearance from the body and (iv) the restriction of PTT/PDT efficiencies for cancer ablation by tissue NIR light penetration depth.

To address these issues, novel and tailored organic nanotheranostic agents with high stability, biodegradability and strong NIR absorption should be developed to satisfy

 

specific diagnostic and therapeutic demands. Some novel dyes and SPs, which possess either high absorption in the second NIR region (>950 nm) or high $^1O_2$ quantum yield with activation by NIR light, should be synthesized and developed into organic nanotheranostic agents to amplify PTT/PDT efficiencies. More importantly, to improve the photostability, biodegradability and biocompatibility of these nanotheranostic agents, some biocompatible polymers, micelles, liposomes and biocompatible groups (ligands, peptides and proteins) should be designed and applied to encapsulate or modify organic materials. New formulation methods to reduce the dimension of organic nanotheranostic agents below 5 nm are also important, since nanoparticles with such a small size have the ability to go through the glomerular capillary wall, and to be cleared from human bodies *via* urinary excretion. Thus, despite the great challenges in translating NIR-absorbing organic nanoparticles into clinical usage, effective strategies to improve their diagnostic and therapeutic performance could be found at the interface of chemistry, nanoscience and biology.

## Conflicts of interest

The authors declare no competing financial interest.

## Acknowledgements

This work was supported by Nanyang Technological University start-up grant (NTU-SUG: M4081627.120), Academic Research Fund Tier 1 from the Singapore Ministry of Education (RG133/15: M4011559, 2017-T1-002-134-RG147/17) and Academic Research Fund Tier 2 from the Ministry of Education in Singapore (MOE2016-T2-1-098).

## References

1 J. P. Celli, B. Q. Spring, I. Rizvi, C. L. Evans, K. S. Samkoe, S. Verma, B. W. Pogue and T. Hasan, *Chem. Rev.*, 2010, **110**, 2795–2838.
2 S. Lal, S. E. Clare and N. J. Halas, *Acc. Chem. Res.*, 2008, **41**, 1842–1851.
3 L. Cheng, C. Wang, L. Z. Feng, K. Yang and Z. Liu, *Chem. Rev.*, 2014, **114**, 10869–10939.
4 H. Y. Liu, D. Chen, L. L. Li, T. L. Liu, L. F. Tan, X. L. Wu and F. Q. Tang, *Angew. Chem., Int. Ed.*, 2011, **50**, 891–895.
5 W. J. Dong, Y. S. Li, D. C. Niu, Z. Ma, J. L. Gu, Y. Chen, W. R. Zhao, X. H. Liu, C. S. Liu and J. L. Shi, *Adv. Mater.*, 2011, **23**, 5392–5397.
6 K. Yang, S. A. Zhang, G. X. Zhang, X. M. Sun, S. T. Lee and Z. A. Liu, *Nano Lett.*, 2010, **10**, 3318–3323.
7 J. T. Robinson, S. M. Tabakman, Y. Y. Liang, H. L. Wang, H. S. Casalongue, D. Vinh and H. J. Dai, *J. Am. Chem. Soc.*, 2011, **133**, 6825–6831.
8 K. Yang, L. L. Hu, X. X. Ma, S. Q. Ye, L. Cheng, X. Z. Shi, C. H. Li, Y. G. Li and Z. Liu, *Adv. Mater.*, 2012, **24**, 1868–1872.
9 L. Cheng, K. Yang, Y. G. Li, J. H. Chen, C. Wang, M. W. Shao, S. T. Lee and Z. Liu, *Angew. Chem., Int. Ed.*, 2011, **50**, 7385–7390.
10 K. Liu, X. Liu, Q. Zeng, Y. Zhang, L. Tu, T. Liu, X. Kong, Y. Wang, F. Cao, S. A. Lambrechts, M. C. Aalders and H. Zhang, *ACS Nano*, 2012, **6**, 4054–4062.
11 S. B. Brown, E. A. Brown and I. Walker, *Lancet Oncol.*, 2004, **5**, 497–508.
12 P. Zhang, W. Steelant, M. Kumar and M. Scholfield, *J. Am. Chem. Soc.*, 2007, **129**, 4526–4527.
13 D. E. Dolmans, D. Fukumura and R. K. Jain, *Nat. Rev. Cancer*, 2003, **3**, 380–387.
14 P. Huang, J. Lin, X. S. Wang, Z. Wang, C. L. Zhang, M. He, K. Wang, F. Chen, Z. M. Li, G. X. Shen, D. X. Cui and X. Y. Chen, *Adv. Mater.*, 2012, **24**, 5104–5110.
15 H. Zhu, J. Li, X. Qi, P. Chen and K. Pu, *Nano Lett.*, 2018, **18**, 586–594.
16 J. Woodcock, J. P. Griffin and R. E. Behrman, *N. Engl. J. Med.*, 2011, **364**, 985–987.
17 X. Yue, Q. Zhang and Z. Dai, *Adv. Drug Delivery Rev.*, 2017, **115**, 155–170.
18 S. J. Wang, P. Huang, L. M. Nie, R. J. Xing, D. B. Liu, Z. Wang, J. Lin, S. H. Chen, G. Niu, G. M. Lu and X. Y. Chen, *Adv. Mater.*, 2013, **25**, 3055–3061.
19 Y. Cheng, A. C. Samia, J. D. Meyers, I. Panagopoulos, B. W. Fei and C. Burda, *J. Am. Chem. Soc.*, 2008, **130**, 10643–10647.
20 W. S. Kuo, C. N. Chang, Y. T. Chang, M. H. Yang, Y. H. Chien, S. J. Chen and C. S. Yeh, *Angew. Chem., Int. Ed.*, 2010, **49**, 2711–2715.
21 S. C. Boca, M. Potara, A. M. Gabudean, A. Juhem, P. L. Baldeck and S. Astilean, *Cancer Lett.*, 2011, **311**, 131–140.
22 R. Di Corato, D. Palumberi, R. Marotta, M. Scotto, S. Carregal-Romero, P. R. Gil, W. J. Parak and T. Pellegrino, *Small*, 2012, **8**, 2731–2742.
23 M. Manikandan, N. Hasan and H. F. Wu, *Biomaterials*, 2013, **34**, 5833–5842.
24 C. P. Wang, X. P. Cai, J. S. Zhang, X. Y. Wang, Y. Wang, H. F. Ge, W. J. Yan, Q. Huang, J. R. Xiao, Q. Zhang and Y. Y. Cheng, *Small*, 2015, **11**, 2080–2086.
25 X. Yi, K. Yang, C. Liang, X. Y. Zhong, P. Ning, G. S. Song, D. L. Wang, C. C. Ge, C. Y. Chen, Z. F. Chai and Z. Liu, *Adv. Funct. Mater.*, 2015, **25**, 4689–4699.
26 S. G. Wang, X. Li, Y. Chen, X. J. Cai, H. L. Yao, W. Gao, Y. Y. Zheng, X. An, J. L. Shi and H. R. Chen, *Adv. Mater.*, 2015, **27**, 2775–2782.
27 J. Liu, X. P. Zheng, L. Yan, L. J. Zhou, G. Tian, W. Y. Yin, L. M. Wang, Y. Liu, Z. B. Hu, Z. J. Gu, C. Y. Chen and Y. L. Zhao, *ACS Nano*, 2015, **9**, 696–707.
28 Y. Yong, X. J. Cheng, T. Bao, M. Zu, L. Yan, W. Y. Yin, C. C. Ge, D. L. Wang, Z. J. Gu and Y. L. Zhao, *ACS Nano*, 2015, **9**, 12451–12463.

29 Z. Q. Chen and G. C. Yin, *Chem. Soc. Rev.*, 2015, **44**, 1083–1100.
30 T. Liu, C. Wang, X. Gu, H. Gong, L. Cheng, X. Z. Shi, L. Z. Feng, B. Q. Sun and Z. Liu, *Adv. Mater.*, 2014, **26**, 3433–3440.
31 H. J. Zhu, Z. C. Lai, Y. Fang, X. Zhen, C. L. Tan, X. Y. Qi, D. Ding, P. Chen, H. Zhang and K. Y. Pu, *Small*, 2017, 1604139.
32 L. Cheng, J. J. Liu, X. Gu, H. Gong, X. Z. Shi, T. Liu, C. Wang, X. Y. Wang, G. Liu, H. Y. Xing, W. B. Bu, B. Q. Sun and Z. Liu, *Adv. Mater.*, 2014, **26**, 1886–1893.
33 G. Tian, X. Zhang, X. P. Zheng, W. Y. Yin, L. F. Ruan, X. D. Liu, L. J. Zhou, L. Yan, S. J. Li, Z. J. Gu and Y. L. Zhao, *Small*, 2014, **10**, 4160–4170.
34 L. S. Lin, Z. X. Cong, J. B. Cao, K. M. Ke, Q. L. Peng, J. H. Gao, H. H. Yang, G. Liu and X. Y. Chen, *ACS Nano*, 2014, **8**, 3876–3883.
35 Q. Chen, L. Z. Feng, J. J. Liu, W. W. Zhu, Z. L. Dong, Y. F. Wu and Z. Liu, *Adv. Mater.*, 2016, **28**, 7129–7136.
36 G. S. Song, J. L. Hao, C. Liang, T. Liu, M. Gao, L. Cheng, J. Q. Hu and Z. Liu, *Angew. Chem., Int. Ed.*, 2016, **55**, 2122–2126.
37 Y. S. Jin, Y. Y. Li, X. B. Ma, Z. B. Zha, L. L. Shi, J. Tian and Z. F. Dai, *Biomaterials*, 2014, **35**, 5795–5804.
38 J. L. Wang and J. J. Qiu, *Sci. Adv. Mater.*, 2015, **7**, 1979–1989.
39 J. L. Wang, J. H. Wei, S. H. Su and J. J. Qiu, *New J. Chem.*, 2015, **39**, 501–507.
40 D. Gopi, E. Shinyjoy and L. Kavitha, *Ceram. Int.*, 2015, **41**, 5454–5463.
41 P. Huang, C. Xu, J. Lin, C. Wang, X. S. Wang, C. L. Zhang, X. J. Zhou, S. W. Guo and D. X. Cui, *Theranostics*, 2011, **1**, 240–250.
42 L. Feng, C. Zhu, H. Yuan, L. Liu, F. Lv and S. Wang, *Chem. Soc. Rev.*, 2013, **42**, 6620–6633.
43 H. Zhu, C. Xie, P. Chen and K. Pu, *Curr. Med. Chem.*, 2017, DOI: 10.2174/0929867324666170921103152.
44 X. Zhen, X. Feng, C. Xie, Y. Zheng and K. Pu, *Biomaterials*, 2017, **127**, 97–106.
45 Y. Jiang and K. Pu, *Small*, 2017, **13**, 1700710.
46 S. M. Sharker, J. E. Lee, S. H. Kim, J. H. Jeong, I. In, H. Lee and S. Y. Park, *Biomaterials*, 2015, **61**, 229–238.
47 M. B. Zheng, P. F. Zhao, Z. Y. Luo, P. Gong, C. F. Zheng, P. F. Zhang, C. X. Yue, D. Y. Gao, Y. F. Ma and L. T. Cai, *ACS Appl. Mater. Interfaces*, 2014, **6**, 6709–6716.
48 E. Crescenzi, L. Varriale, M. Iovino, A. Chiaviello, B. M. Veneziani and G. Palumbo, *Mol. Cancer Ther.*, 2004, **3**, 537–544.
49 C. Q. Zhao, F. U. Rehman, Y. L. Yang, X. Q. Li, D. Zhang, H. Jiang, M. Selke, X. M. Wang and C. Y. Liu, *Sci. Rep.*, 2015, **5**, 11518.
50 J. F. Lovell, C. S. Jin, E. Huynh, H. L. Jin, C. Kim, J. L. Rubinstein, W. C. W. Chan, W. G. Cao, L. V. Wang and G. Zheng, *Nat. Mater.*, 2011, **10**, 324–332.
51 X. L. Liang, Y. Y. Li, X. D. Li, L. J. Jing, Z. J. Deng, X. L. Yue, C. H. Li and Z. F. Dai, *Adv. Funct. Mater.*, 2015, **25**, 1451–1462.
52 Q. Miao, C. Xie, X. Zhen, Y. Lyu, H. Duan, X. Liu, J. V. Jokerst and K. Pu, *Nat. Biotechnol.*, 2017, **35**, 1102–1110.
53 C. Yin, H. Zhu, C. Xie, L. Zhang, P. Chen, Q. Fan, W. Huang and K. Pu, *Adv. Funct. Mater.*, 2017, **27**, 1700493.
54 X. Zhen, C. Zhang, C. Xie, Q. Miao, K. L. Lim and K. Pu, *ACS Nano*, 2016, **10**, 6400–6409.
55 H. J. Zhu, Y. Fang, X. Zhen, N. Wei, Y. Gao, K. Q. Luo, C. J. Xu, H. W. Duan, D. Ding, P. Chen and K. Y. Pu, *Chem. Sci.*, 2016, **7**, 5118–5125.
56 Y. Lyu, X. Zhen, Y. S. Miao and K. Y. Pu, *ACS Nano*, 2017, **11**, 358–367.
57 C. Xie, X. Zhen, Q. Lei, R. Ni and K. Pu, *Adv. Funct. Mater.*, 2017, **27**, 1605397.
58 Y. Lyu, D. Cui, H. Sun, Y. Miao, H. Duan and K. Pu, *Angew. Chem., Int. Ed.*, 2017, **56**, 9155–9159.
59 Y. Lyu, C. Xie, S. A. Chechetka, E. Miyako and K. Pu, *J. Am. Chem. Soc.*, 2016, **138**, 9049–9052.
60 Q. Chen, J. Wen, H. Li, Y. Xu, F. Liu and S. Sun, *Biomaterials*, 2016, **106**, 144–166.
61 Y. Ma, J. Huang, S. Song, H. Chen and Z. Zhang, *Small*, 2016, **12**, 4936–4954.
62 P. Bhattarai and Z. Dai, *Adv. Healthcare Mater.*, 2017, **6**, 1700262.
63 M. Abbas, Q. Zou, S. Li and X. Yan, *Adv. Mater.*, 2017, **29**, 1605621.
64 J. Li, J. Rao and K. Pu, *Biomaterials*, 2017, **155**, 217–235.
65 J. Wang, W. Tao, X. Chen, O. C. Farokhzad and G. Liu, *Theranostics*, 2017, **7**, 3915–3919.
66 B. Zhou, Y. Li, G. Niu, M. Lan, Q. Jia and Q. Liang, *ACS Appl. Mater. Interfaces*, 2016, **8**, 29899–29905.
67 W. H. Jian, T. W. Yu, C. J. Chen, W. C. Huang, H. C. Chiu and W. H. Chiang, *Langmuir*, 2015, **31**, 6202–6210.
68 X. Zheng, F. Zhou, B. Wu, W. R. Chen and D. Xing, *Mol. Pharm.*, 2012, **9**, 514–522.
69 C. W. Hsiao, E. Y. Chuang, H. L. Chen, D. Wan, C. Korupalli, Z. X. Liao, Y. L. Chiu, W. T. Chia, K. J. Lin and H. W. Sung, *Biomaterials*, 2015, **56**, 26–35.
70 B. Bahmani, Y. Guerrero, D. Bacon, V. Kundra, V. I. Vullev and B. Anvari, *Lasers Surg. Med.*, 2014, **46**, 582–592.
71 Y. Hong, W. Cho, J. Kim, S. Hwng, E. Lee, D. Heo, M. Ku, J. S. Suh, J. Yang and J. H. Kim, *Nanotechnology*, 2016, **27**, 185104.
72 X. J. Song, Q. Chen and Z. Liu, *Nano Res.*, 2015, **8**, 340–354.
73 J. Yang, J. Choi, D. Bang, E. Kim, E. K. Lim, H. Park, J. S. Suh, K. Lee, K. H. Yoo, E. K. Kim, Y. M. Huh and S. Haam, *Angew. Chem., Int. Ed.*, 2011, **50**, 441–444.
74 J. Zhou, Z. Lu, X. Zhu, X. Wang, Y. Liao, Z. Ma and F. Li, *Biomaterials*, 2013, **34**, 9584–9592.
75 K. Yang, H. Xu, L. Cheng, C. Sun, J. Wang and Z. Liu, *Adv. Mater.*, 2012, **24**, 5586–5592.

 

76 M. Chen, X. Fang, S. Tang and N. Zheng, *Chem. Commun.*, 2012, **48**, 8934–8936.
77 K. Ke, L. Lin, H. Liang, X. Chen, C. Han, J. Li and H. H. Yang, *Chem. Commun.*, 2015, **51**, 6800–6803.
78 J. Geng, C. Sun, J. Liu, L. D. Liao, Y. Yuan, N. Thakor, J. Wang and B. Liu, *Small*, 2015, **11**, 1603–1610.
79 S. Li, X. Wang, R. Hu, H. Chen, M. Li, J. Wang, Y. Wang, L. Liu, F. Lv, X. Liang and S. Wang, *Chem. Mater.*, 2017, **1353**, 1531–6386.
80 B. Guo, G. Feng, P. N. Manghnani, X. Cai, J. Liu, W. Wu, S. Xu, X. Cheng, C. Teh and B. Liu, *Small*, 2016, **12**, 6243–6254.
81 Y. Cao, J. Dou, N. Zhao, S. Zhang, Y. Zheng, J. Zhang, J. Wang, J. Pei and Y. Wang, *Chem. Mater.*, 2017, **29**, 718–725.
82 L. Cheng, W. He, H. Gong, C. Wang, Q. Chen, Z. Cheng and Z. Liu, *Adv. Funct. Mater.*, 2017, **23**, 5893–5902.
83 Q. Chen, C. Wang, Z. Zhan, W. He, Z. Cheng, Y. Li and Z. Liu, *Biomaterials*, 2014, **35**, 8206–8214.
84 C. Yue, P. Liu, M. Zheng, P. Zhao, Y. Wang, Y. Ma and L. Cai, *Biomaterials*, 2013, **34**, 6853–6861.
85 G. Chen, K. Wang, Y. Zhou, L. Ding, A. Ullah, Q. Hu, M. Sun and D. Oupicky, *ACS Appl. Mater. Interfaces*, 2016, **8**, 25087–25095.
86 Y. Chen, Z. Li, H. Wang, Y. Wang, H. Han, Q. Jin and J. Ji, *ACS Appl. Mater. Interfaces*, 2016, **8**, 6852–6858.
87 Y. Li, G. Liu, J. Ma, J. Lin, H. Lin, G. Su, D. Chen, S. Ye, X. Chen, X. Zhu and Z. Hou, *J. Controlled Release*, 2017, **258**, 95–107.
88 X. Qiu, L. Xu, Y. Zhang, A. Yuan, K. Wang, X. Zhao, J. Wu, H. Guo and Y. Hu, *Mol. Pharm.*, 2016, **13**, 829–838.
89 H. Han, S. Zhang, Y. Wang, T. Chen, Q. Jin, Y. Chen, Z. Li and J. Ji, *Polymer*, 2016, **82**, 255–261.
90 Y. Kuang, K. Zhang, Y. Cao, X. Chen, K. Wang, M. Liu and R. Pei, *ACS Appl. Mater. Interfaces*, 2017, **9**, 12217–12226.
91 X. Zheng, D. Xing, F. Zhou, B. Wu and W. Chen, *Pharmaceutics*, 2011, **8**, 447–456.
92 L. Wu, S. Fang, S. Shi, J. Deng, B. Liu and L. Cai, *Biomacromolecules*, 2013, **14**, 3027–3033.
93 J. Zhang, X. Zhen, P. K. Upputuri, M. Pramanik, P. Chen and K. Pu, *Adv. Mater.*, 2016, **29**, 1604764.
94 K. Y. Pu, A. J. Shuhendler, J. V. Jokerst, J. G. Mei, S. S. Gambhir, Z. N. Bao and J. H. Rao, *Nat. Nanotechnol.*, 2014, **9**, 233–239.
95 D. Cui, C. Xie, Y. Lyu, X. Zhen and K. Pu, *J. Mater. Chem. B*, 2017, **5**, 4406–4409.
96 C. Xie, X. Zhen, Y. Lyu and K. Pu, *Adv. Mater.*, 2017, **29**, 1703693.
97 Y. Jiang, P. K. Upputuri, C. Xie, Y. Lyu, L. Zhang, Q. Xiong, M. Pramanik and K. Pu, *Nano Lett.*, 2017, **17**, 4964–4969.
98 S. Huang, P. K. Upputuri, H. Liu, M. Pramanik and M. F. Wang, *J. Mater. Chem. B*, 2016, **4**, 1696–1703.
99 J. Qi, Y. Fang, R. T. K. Kwok, X. Zhang, X. Hu, J. W. Y. Lam, D. Ding and B. Z. Tang, *ACS Nano*, 2017, **11**, 7177–7188.
100 Q. Chen, X. Liu, J. Zeng, Z. Cheng and Z. Liu, *Biomaterials*, 2016, **98**, 23–30.
101 S. Guha, G. K. Shaw, T. M. Mitcham, R. R. Bouchard and B. D. Smith, *Chem. Commun.*, 2016, **52**, 120–123.
102 Q. Zou, M. Abbas, L. Zhao, S. Li, G. Shen and X. Yan, *J. Am. Chem. Soc.*, 2017, **139**, 1921–1927.
103 C. Yin, X. Zhen, H. Zhao, Y. Tang, Y. Ji, Y. Lyu, Q. Fan, W. Huang and K. Pu, *ACS Appl. Mater. Interfaces*, 2017, **9**, 12332–12339.
104 C. Xie, P. K. Upputuri, X. Zhen, M. Pramanik and K. Pu, *Biomaterials*, 2017, **119**, 1–8.
105 Q. Miao, Y. Lyu, D. Ding and K. Pu, *Adv. Mater.*, 2016, **28**, 3662–3668.
106 C. Yin, X. Zhen, Q. Fan, W. Huang and K. Pu, *ACS Nano*, 2017, **11**, 4174–4182.
107 S. Zhang, W. Guo, J. Wei, C. Li, X. J. Liang and M. Yin, *ACS Nano*, 2017, **11**, 3797–3805.
108 Y. Lyu, Y. Fang, Q. Miao, X. Zhen, D. Ding and K. Pu, *ACS Nano*, 2016, **10**, 4472–4481.
109 X. Cai, X. Liu, L. D. Liao, A. Bandla, J. M. Ling, Y. H. Liu, N. Thakor, G. C. Bazan and B. Liu, *Small*, 2016, **12**, 4873–4880.
110 B. Guo, Z. Sheng, D. Hu, A. Li, S. Xu, P. N. Manghnani, C. Liu, L. Guo, H. Zheng and B. Liu, *ACS Nano*, 2017, **11**, 10124–10134.
111 D. Li, G. Zhang, W. Xu, J. Wang, Y. Wang, L. Qiu, J. Ding and X. Yang, *Theranostics*, 2017, **7**, 4029–4040.
112 L. Guo, W. Liu, G. Niu, P. Zhang, X. Zheng, Q. Jia, H. Zhang, J. Ge and P. Wang, *J. Mater. Chem. B*, 2017, **5**, 2832–2839.
113 Y. Yuan, H. B. Sun, S. C. Ge, M. J. Wang, H. X. Zhao, L. Wang, L. N. An, J. Zhang, H. F. Zhang, B. Hu, J. F. Wang and G. L. Liang, *ACS Nano*, 2015, **9**, 761–768.
114 X. J. Song, H. Gong, T. Liu, L. Cheng, C. Wang, X. Q. Sun, C. Liang and Z. Liu, *Small*, 2014, **10**, 4362–4370.
115 L. J. Jing, X. L. Liang, X. D. Li, L. Lin, Y. B. Yang, X. L. Yue and Z. F. Dai, *Theranostics*, 2014, **4**, 858–871.
116 Y. Yang, J. Liu, C. Liang, L. Feng, T. Fu, Z. Dong, Y. Chao, Y. Li, G. Lu, M. Chen and Z. Liu, *ACS Nano*, 2016, **10**, 2774–2781.
117 Z. B. Zha, S. M. Wang, S. H. Zhang, E. Z. Qu, H. T. Ke, J. R. Wang and Z. F. Dai, *Nanoscale*, 2013, **5**, 3216–3219.
118 Z. B. Zha, J. R. Wang, S. H. Zhang, S. M. Wang, E. Qu, Y. Y. Zhang and Z. F. Dai, *Biomaterials*, 2014, **35**, 287–293.
119 H. T. Ke, J. R. Wang, Z. F. Dai, Y. S. Jin, E. Z. Qu, Z. W. Xing, C. X. Guo, X. L. Yue and J. B. Liu, *Angew. Chem., Int. Ed.*, 2011, **50**, 3017–3021.
120 Y. W. Hao, B. X. Zhang, C. X. Zheng, R. Ji, X. Y. Ren, F. F. Guo, S. L. Sun, J. J. Shi, H. L. Zhang, Z. Z. Zhang, L. Wang and Y. Zhang, *J. Controlled Release*, 2015, **220**, 545–555.
121 H. Deng, Y. Q. Zhong, M. H. Du, Q. J. Liu, Z. M. Fan, F. Y. Dai and X. Zhang, *Theranostics*, 2014, **4**, 904–918.
122 J. B. Qin, Z. Y. Peng, B. Li, K. C. Ye, Y. X. Zhang, F. K. Yuan, X. R. Yang, L. J. Huang, J. Q. Hu and X. W. Lu, *Nanoscale*, 2015, **7**, 13991–14001.
123 W. Guo, C. Guo, N. Zheng, T. Sun and S. Liu, *Adv. Mater.*, 2017, **29**, 1604157.

124 Y. Liu, K. Ai, J. Liu, M. Deng, Y. He and L. Lu, *Adv. Mater.*, 2013, **25**, 1353–1359.
125 T. Lee, D. Bang, Y. Park, S. H. Kim, J. Choi, J. Park, D. Kim, E. Kim, J. S. Suh, Y. M. Huh and S. Haam, *Adv. Healthcare Mater.*, 2014, **3**, 1408–1414.
126 J. Wang, F. Guo, M. Yu, L. Liu, F. Tan, R. Yan and N. Li, *J. Controlled Release*, 2016, **237**, 23–34.
127 L. Tang, F. Zhang, F. Yu, W. Sun, M. Song, X. Chen, X. Zhang and X. Sun, *Biomaterials*, 2017, **129**, 28–36.
128 W. Lin, Y. Li, W. Zhang, S. Liu, Z. Xie and X. Jing, *ACS Appl. Mater. Interfaces*, 2016, **8**, 24426–24432.
129 M. Zhu, Z. Sheng, Y. Jia, D. Hu, X. Liu, X. Xia, C. Liu, P. Wang, X. Wang and H. Zheng, *ACS Appl. Mater. Interfaces*, 2017, **9**, 39249–39258.
130 S. Li, Z. Sun, G. Deng, X. Meng, W. Li, D. Ni, J. Zhang, P. Gong and L. Cai, *Biomater. Sci.*, 2017, **5**, 1122–1129.
131 X. Liang, L. Fang, X. Li, X. Zhang and F. Wang, *Biomaterials*, 2017, **132**, 72–84.
132 D. Hu, C. Liu, L. Song, H. Cui, G. Gao, P. Liu, Z. Sheng and L. Cai, *Nanoscale*, 2016, **8**, 17150–17158.
133 W. Cai, H. Gao, C. Chu, X. Wang, J. Wang, P. Zhang, G. Lin, W. Li, G. Liu and X. Chen, *ACS Appl. Mater. Interfaces*, 2017, **9**, 2040–2051.
134 Q. Chen, C. Liang, X. Wang, J. He, Y. Li and Z. Liu, *Biomaterials*, 2014, **35**, 9355–9362.
135 C. L. Peng, Y. H. Shih, P. C. Lee, T. M. Hsieh, T. Y. Luo and M. J. Shieh, *ACS Nano*, 2011, **5**, 5594–5607.
136 Y. H. Shih, T. Y. Luo, P. F. Chiang, C. J. Yao, W. J. Lin, C. L. Peng and M. J. Shieh, *J. Controlled Release*, 2017, **258**, 196–207.
137 S. Shi, Y. Liu, Y. Chen, Z. Zhang, Y. Ding, Z. Wu, J. Yin and L. Nie, *Theranostics*, 2016, **6**, 2170–2182.
138 Y. I. Chen, C. L. Peng, P. C. Lee, M. H. Tsai, C. Y. Lin, Y. H. Shih, M. F. Wei, T. Y. Luo and M. J. Shieh, *Adv. Healthcare Mater.*, 2015, **4**, 892–902.
139 Y. Zhang, C. Teh, M. Li, C. Ang, S. Tan, Q. Qu, V. Korzh and L. Zhao, *Chem. Mater.*, 2016, **28**, 7039–7705.
140 M. B. Zheng, C. X. Yue, Y. F. Ma, P. Gong, P. F. Zhao, C. F. Zheng, Z. H. Sheng, P. F. Zhang, Z. H. Wang and L. T. Cai, *ACS Nano*, 2013, **7**, 2056–2067.
141 Y. Li, G. Liu, J. Ma, J. Lin, H. Lin, G. Su, D. Chen, S. Ye, X. Chen, X. Zhu and Z. Hou, *J. Controlled Release*, 2017, **258**, 95–107.
142 P. R. Jheng, K. Y. Lu, S. H. Yu and F. L. Mi, *Colloids Surf., B*, 2015, **136**, 402–412.
143 Q. Chen, C. Liang, C. Wang and Z. Liu, *Adv. Mater.*, 2015, **27**, 903–910.
144 X. Song, R. Zhang, C. Liang, Q. Chen, H. Gong and Z. Liu, *Biomaterials*, 2015, **57**, 84–92.
145 Y. Han, J. Li, M. Zan, S. Luo, Z. Ge and S. Liu, *Polym. Chem.*, 2014, **5**, 3707–3718.
146 Y. Yuan, Z. Wang, P. Cai, J. Liu, L. D. Liao, M. Hong, X. Chen, N. Thakor and B. Liu, *Nanoscale*, 2015, **7**, 3067–3076.
147 H. Liu, K. Wang, C. Yang, S. Huang and M. Wang, *Colloids Surf., B*, 2017, **157**, 398–406.
148 Y. Jiang, D. Cui, Y. Fang, X. Zhen, P. K. Upputuri, M. Pramanik, D. Ding and K. Pu, *Biomaterials*, 2017, **145**, 168–177.
149 D. D. Li, J. X. Wang, Y. Ma, H. S. Qian, D. Wang, L. Wang, G. Zhang, L. Qiu, Y. C. Wang and X. Z. Yang, *ACS Appl. Mater. Interfaces*, 2016, **8**, 19312–19320.
150 Y. Cao, J. Yi, X. Yang, L. Liu, C. Yu, Y. Huang, L. Sun, Y. Bao and Y. Li, *Biomacromolecules*, 2017, **18**, 2306–2314.
151 T. Cao, Y. Wu, G. Wang, J. Yi, C. Yu, Y. Huang, L. Sun, Y. Bao and Y. Li, *J. Mater. Chem. C*, 2017, **5**, 5479–5487.
152 Y. D. Zhu, S. P. Chen, H. Zhao, Y. Yang, X. Q. Chen, J. Sun, H. S. Fan and X. D. Zhang, *ACS Appl. Mater. Interfaces*, 2016, **8**, 34209–34217.
153 D. Park, K. O. Ahn, K. C. Jeong and Y. Choi, *Nanotechnology*, 2016, **27**, 185102.
154 C. V. Synatschke, T. Nomoto, H. Cabral, M. Fortsch, K. Toh, Y. Matsumoto, K. Miyazaki, A. Hanisch, F. H. Schacher, A. Kishimura, N. Nishiyama, A. H. Muller and K. Kataoka, *ACS Nano*, 2014, **8**, 1161–1172.
155 A. Yuan, B. Yang, J. Wu, Y. Hu and X. Ming, *Acta Biomater.*, 2015, **21**, 63–73.
156 H. Y. Yoon, H. Koo, K. Y. Choi, S. J. Lee, K. Kim, I. C. Kwon, J. F. Leary, K. Park, S. H. Yuk, J. H. Park and K. Choi, *Biomaterials*, 2012, **33**, 3980–3989.
157 Y. Zhang, T. Lv, H. Zhang, X. Xie, Z. Li, H. Chen and Y. Gao, *Biomacromolecules*, 2017, **18**, 2146–2160.
158 H. R. Jia, Y. W. Jiang, Y. X. Zhu, Y. H. Li, H. Y. Wang, X. Han, Z. W. Yu, N. Gu, P. Liu, Z. Chen and F. G. Wu, *J. Controlled Release*, 2017, **255**, 231–241.
159 H. Ren, J. Liu, F. Su, S. Ge, A. Yuan, W. Dai, J. Wu and Y. Hu, *ACS Appl. Mater. Interfaces*, 2017, **9**, 3463–3473.
160 L. Liu, Z. Ruan, T. Li, P. Yuan and L. Yan, *Biomater. Sci.*, 2016, **4**, 1638–1645.
161 L. Huang, Z. Li, Y. Zhao, J. Yang, Y. Yang, A. I. Pendharkar, Y. Zhang, S. Kelmar, L. Chen, W. Wu, J. Zhao and G. Han, *Adv. Mater.*, 2017, 29.
162 L. Guo, J. Ge, Q. Liu, Q. Jia, H. Zhang, W. Liu, G. Niu, S. Liu, J. Gong, S. Hackbarth and P. Wang, *Adv. Healthcare Mater.*, 2017, **6**, 1601431.
163 H. Zhu, Y. Fang, Q. Miao, X. Qi, D. Ding, P. Chen and K. Pu, *ACS Nano*, 2017, **11**, 8998–9009.
164 K. Han, S. B. Wang, Q. Lei, J. Y. Zhu and X. Z. Zhang, *ACS Nano*, 2015, **9**, 10268–10277.
165 L. Cheng, A. Kamkaew, H. Sun, D. Jiang, H. F. Valdovinos, H. Gong, C. G. England, S. Goel, T. E. Barnhart and W. Cai, *ACS Nano*, 2016, **10**, 7721–7730.
166 Y. Huang, F. Qiu, L. Shen, D. Chen, Y. Su, C. Yang, B. Li, D. Yan and X. Zhu, *ACS Nano*, 2016, **10**, 10489–10499.
167 H. Tong, Y. Chen, Z. Li, H. Li, T. Chen, Q. Jin and J. Ji, *Small*, 2016, **12**, 6223–6232.
168 K. Liu, R. Xing, Q. Zou, G. Ma, H. Mohwald and X. Yan, *Angew. Chem., Int. Ed.*, 2016, **55**, 3036–3039.
169 D. Wang, T. Wang, J. Liu, H. Yu, S. Jiao, B. Feng, F. Zhou, Y. Fu, Q. Yin, P. Zhang, Z. Zhang, Z. Zhou and Y. Li, *Nano Lett.*, 2016, **16**, 5503–5513.

 

170 W. Li, C. Zheng, Z. Pan, C. Chen, D. Hu, G. Gao, S. Kang, H. Cui, P. Gong and L. Cai, *Biomaterials*, 2016, **101**, 10–19.
171 K. E. Park, Y. W. Noh, A. Kim and Y. T. Lim, *Carbohydr. Polym.*, 2017, **157**, 476–483.
172 H. Wu, H. Wang, H. Liao, Y. Lv, X. Song, X. Ma and M. Tan, *Adv. Healthcare Mater.*, 2016, **5**, 311–318.
173 O. Taratula, C. Schumann, M. A. Naleway, A. J. Pang and K. J. Chon, *Mol. Pharm.*, 2013, **10**, 3946–3958.
174 Z. Ruan, L. Liu, W. Jiang, S. Li, Y. Wang and L. Yan, *Biomater. Sci.*, 2017, **5**, 313–321.
175 Y. Yuan, J. Liu and B. Liu, *Angew. Chem., Int. Ed.*, 2014, **53**, 7163–7168.
176 J. C. Bremner, G. E. Adams, J. K. Pearson, J. M. Sansom, I. J. Stratford, J. Bedwell, S. G. Bown, A. J. MacRobert and D. Phillips, *Br. J. Cancer*, 1992, **66**, 1070–1076.
177 L. Feng, L. Cheng, Z. Dong, D. Tao, T. E. Barnhart, W. Cai, M. Chen and Z. Liu, *ACS Nano*, 2017, **11**, 927–937.
178 S. Y. Li, H. Cheng, W. X. Qiu, L. Zhang, S. S. Wan, J. Y. Zeng and X. Z. Zhang, *Biomaterials*, 2017, **142**, 149–161.
179 Y. Wang, Y. Xie, J. Li, Z. H. Peng, Y. Sheinin, J. Zhou and D. Oupicky, *ACS Nano*, 2017, **11**, 2227–2238.
180 C. Chu, H. Lin, H. Liu, X. Wang, J. Wang, P. Zhang, H. Gao, C. Huang, Y. Zeng, Y. Tan, G. Liu and X. Chen, *Adv. Mater.*, 2017, **29**, 1605928.
181 J. Kim, H. R. Cho, H. Jeon, D. Kim, C. Song, N. Lee, S. H. Choi and T. Hyeon, *J. Am. Chem. Soc.*, 2017, **139**, 10992–10995.
182 Q. Chen, L. Feng, J. Liu, W. Zhu, Z. Dong, Y. Wu and Z. Liu, *Adv. Mater.*, 2016, **28**, 7129–7136.
183 C. S. Jin, J. F. Lovell, J. Chen and G. Zheng, *ACS Nano*, 2013, **7**, 2541–2550.
184 Z. Guo, Y. Zou, H. He, J. Rao, S. Ji, X. Cui, H. Ke, Y. Deng, H. Yang, C. Chen, Y. Zhao and H. Chen, *Adv. Mater.*, 2016, **28**, 10155–10164.
185 O. Taratula, C. Schumann, T. Duong and K. L. Taylor, *Nanoscale*, 2015, **7**, 3888–3902.
186 L. Li, Y. Liu, P. Hao, Z. Wang, L. Fu, Z. Ma and J. Zhou, *Biomaterials*, 2015, **41**, 132–140.
187 T. H. Tran, H. T. Nguyen, T. T. Phuong Tran, S. K. Ku, J. H. Jeong, H. G. Choi, C. S. Yong and J. O. Kim, *Nanomedicine*, 2017, DOI: 10.2217/nnm-2016-0438.
188 D. Zhang, M. Wu, Y. Zeng, L. Wu, Q. Wang, X. Han, X. Liu and J. Liu, *ACS Appl. Mater. Interfaces*, 2015, **7**, 8176–8187.
189 N. Zhang, F. Zhao, Q. Zou, Y. Li, G. Ma and X. Yan, *Small*, 2016, **12**, 5936–5943.
190 W. Miao, H. Kim, V. Gujrati, J. Y. Kim, H. Jon, Y. Lee, M. Choi, J. Kim, S. Lee, D. Y. Lee, S. Kang and S. Jon, *Theranostics*, 2016, **6**, 2367–2379.
191 F. Yan, H. Wu, H. Liu, Z. Deng, W. Duan, X. Liu and H. Zheng, *J. Controlled Release*, 2016, **224**, 217–228.
192 C. Jiang, H. Cheng, A. Yuan, X. Tang, J. Wu and Y. Hu, *Acta Biomater.*, 2015, **14**, 61–69.
193 A. Yuan, X. Qiu, X. Tang, W. Liu, J. Wu and Y. Hu, *Biomaterials*, 2015, **51**, 184–193.
194 O. Taratula, B. Doddapaneni, C. Schumann, X. Li, S. Bracha, M. Milovancev, A. Alani and O. Taratula, *Chem. Mater.*, 2015, **27**, 6155–6165.
195 G. Feng, Y. Fang, J. Liu, J. Geng, D. Ding and B. Liu, *Small*, 2017, **13**, 1602807.
196 Q. Tang, W. Xiao, C. Huang, W. Si, J. Shao, W. Huang, P. Chen, Q. Zhang and X. Dong, *Chem. Mater.*, 2017, **29**, 5216–5224.
197 Q. Tang, W. Si, C. Huang, K. Ding, W. Huang, P. Chen, Q. Zhang and X. Dong, *J. Mater. Chem. B*, 2017, **5**, 1566–1573.
198 Y. Cai, P. Liang, Q. Tang, X. Yang, W. Si, W. Huang, Q. Zhang and X. Dong, *ACS Nano*, 2017, **11**, 1054–1063.
199 M. Guo, H. Mao, Y. Li, A. Zhu, H. He, H. Yang, Y. Wang, X. Tian, C. Ge, Q. Peng, X. Wang, X. Yang, X. Chen, G. Liu and H. Chen, *Biomaterials*, 2014, **35**, 4656–4666.
200 Z. Sheng, D. Hu, M. Zheng, P. Zhao, H. Liu, D. Gao, P. Gong, G. Gao, P. Zhang, Y. Ma and L. Cai, *ACS Nano*, 2014, **8**, 12310–12322.
201 L. Feng, D. Tao, Z. Dong, Q. Chen, Y. Chao, Z. Liu and M. Chen, *Biomaterials*, 2017, **127**, 13–24.
202 L. Guo, G. Niu, X. Zheng, J. Ge, W. Liu, Q. Jia, P. Zhang, H. Zhang and P. Wang, *Adv. Sci.*, 2017, **4**, 1700085.
203 W. Yang, J. Noh, H. Park, S. Gwon, B. Singh, C. Song and D. Lee, *Biomaterials*, 2017, **154**, 48–59.
204 D. Zhang, M. Wu, Y. Zeng, N. Liao, Z. Cai, G. Liu, X. Liu and J. Liu, *J. Mater. Chem. B*, 2016, **4**, 589–599.
205 A. Gizzatov, J. Key, S. Aryal, J. Ananta, A. Cervadoro, A. L. Palange, M. Fasano, C. Stigliano, M. Zhong, D. Di Mascolo, A. Guven, E. Chiavazzo, P. Asinari, X. Liu, M. Ferrari, L. J. Wilson and P. Decuzzi, *Adv. Funct. Mater.*, 2014, **24**, 4584–4594.
206 X. Liu, G. Yang, L. Zhang, Z. Liu, Z. Cheng and X. Zhu, *Nanoscale*, 2016, **8**, 15323–15339.
207 C. Huang, C. Chu, X. Wang, H. Lin, J. Wang, Y. Zeng, W. Zhu, Y. J. Wang and G. Liu, *Biomater. Sci.*, 2017, **5**, 1512–1516.
208 X. Song, C. Liang, H. Gong, Q. Chen, C. Wang and Z. Liu, *Small*, 2015, **11**, 3932–3941.
209 H. Gong, Z. L. Dong, Y. M. Liu, S. N. Yin, L. Cheng, W. Y. Xi, J. Xiang, K. Liu, Y. G. Li and Z. Liu, *Adv. Funct. Mater.*, 2014, **24**, 6492–6502.
210 H. Gong, L. Cheng, J. Xiang, H. Xu, L. Feng, X. Shi and Z. Liu, *Adv. Funct. Mater.*, 2013, **23**, 6059–6067.
211 Y. Luo, H. Wu, C. Feng, K. Xiao, X. Yang, Q. Liu, T. Y. Lin, H. Zhang, J. H. Walton, Y. Ajena, Y. Hu, K. S. Lam and Y. Li, *Theranostics*, 2017, **7**, 3901–3914.
212 W. Li, J. Peng, L. Tan, J. Wu, K. Shi, Y. Qu, X. Wei and Z. Qian, *Biomaterials*, 2016, **106**, 119–133.
213 T. Wang, D. Wang, H. Yu, M. Wang, J. Liu, B. Feng, F. Zhou, Q. Yin, Z. Zhang, Y. Huang and Y. Li, *ACS Nano*, 2016, **10**, 3496–3508.